RATIONAL DESIGN OF ORGANOPHOSPHORUS HYDROLASE FOR THE DEGRADATION AND DETECTION OF NEUROTOXIC PESTICIDES AND CHEMICAL WARFARE AGENTS

A Dissertation

by

TONY ELVERN REEVES

Submitted to the Office of Graduate Studies of
Texas A&M University
in partial fulfillment of the requirements for the degree of

DOCTOR OF PHILOSOPHY

May 2006

Major Subject: Biochemistry

RATIONAL DESIGN OF ORGANOPHOSPHORUS HYDROLASE FOR THE DEGRADATION AND DETECTION OF NEUROTOXIC PESTICIDES AND CHEMICAL WARFARE AGENTS

A Dissertation

by

TONY ELVERN REEVES

Submitted to the Office of Graduate Studies of
Texas A&M University
in partial fulfillment of the requirements
for the degree of

DOCTOR OF PHILOSOPHY

Approved by:

Chair of Committee, James Wild
Committee Members, Evelyn Castiglioni
Janet Grimsley
Paul Lindahl
Martin Scholtz
Head of Department, Greg Reinhart

May 2006

Major Subject: Biochemistry

ABSTRACT

Rational Design of Organophosphorus Hydrolase for the Degradation and Detection of Neurotoxic Pesticides and Chemical Warfare Agents. (May 2006)

Tony Elvern Reeves, B.S.; M.S., Tarleton State University

Chair of Advisory Committee: Dr. James R. Wild

It is critical to consider the balance between the catalytic capabilities of an enzyme and the inherent structural stability of the protein when developing enzymes for specific applications. Rational site directed mutagenesis has been used to explore the role of residues 254 and 257 in the global stability and catalytic specificities of organophosphorus hydrolase (OPH, EC 3.1.8.1). Substitution of residues H254 and H257, which are located near the active site, had a marked effect on both the global stability and substrate specificity of the enzyme. For example, the ΔG_T for the double mutation Co^{2+} H254R H257L (RL) enzyme variant was 19.6 kcal/mol, 5.7 kcal/mol less than that of the wild type enzyme. At the same time, the altered enzyme was catalytically more effective against VX and VR (Russian VX), as compared to the wild type enzyme. Limited proteolysis verified the importance of residues 254 and 257 for functional stability, evidenced by enhanced resistance to irreversible unfolding associated with thermal denaturation. It has been possible to construct third generation OPH variants, which are more stable than the wild type enzyme, with a 10 °C increase in the apparent melting temperature ($T_{M\ app}$), yet retained desirable catalytic properties. It appeared that aromatic stacking and cation-π interactions involving near active site

residues not only affected activity but significantly contributed to the chemical and thermal stability of OPH.

Rational design was used to develop an enzyme with an optimized orientation on a catalytically active biosensor surface. In these studies, lysine side chains located on the surface of OPH were used to create attachment sites to a surface plasmon resonance sensor resulting in an ensemble of enzyme orientations. Some of these orientations could be functionally restrictive if the active site is oriented toward the sensor surface. Substitution of a lysine near the active site resulted in 20% more activity with 53% less enzyme immobilized, thus increasing the specific activity of the decorated surface 2.5 fold.

DEDICATION

This dissertation would not have been possible without the love and support of my family.

ACKNOWLEDGEMENTS

I am grateful for the help and support of everybody that contributed to my research. I would like to thank Dr. Wild, a teacher and friend, for giving me the freedom to pursue the things that I found most interesting, and to go outside the lab and work with friends and colleagues. It truly made my learning experience great.

I owe a tremendous amount of my success to Dr. Janet Grimsley, for getting me started and keeping me on track.

I would like to thank all the graduate students and undergraduates that worked with me. Dr. Shane Gold, Dr. Mauricio Rodriquez, Dr. Scott Pinkerton, David Armstrong, Rory Kern, Leamon Viveros, Jess Miller, Claire Rowe, Elizabeth Sherwood and Lisa Torres.

Dr. Melinda Wales, her leadership in the lab was invaluable and her help was indispensable. Thank you.

Finally I would like to thank Dr. Alex Simonian and Sheetal Paliwal for their help in accomplishing the sensor component of this dissertation.

TABLE OF CONTENTS

Page

Page

LIST OF FIGURES

Figure Page

LIST OF TABLES

INTRODUCTION

History of organophosphorus chemical warfare agents

Organophosphorus (OP) compounds have been known and used as insecticides and chemical warfare agents (CWA) since the early 1800's. Produced by the reaction of alcohols and phosphoric acid, the use of toxic chemicals in battle was considered non-chivalrous throughout most of the Renaissance period. As early as 1854, Phillipe de Clermont presented a description of the synthesis of tetraethylpyrophosphate at the French Academy of Sciences, which included recognizing its bitter taste as a method to detect its presence (1). In 1932, Willy Lang of Germany reported the synthesis of OP compounds and studied their toxic properties (2). Continuing these studies, Gerhard Schrader, working at Bayer AG in Germany, synthesized the neurotoxic insecticide parathion, the predecessor to the G series of chemical warfare agents (tabun, soman and sarin) (3). By the end of WWII, American and British scientists were actively synthesizing new organophosphorus compounds, such as diisopropyl fluorophosphonates (DFP) (4) and, by the early 1950's, British scientists had developed VX, one of the most neurotoxic OP known. In order to stay abreast of the burgeoning chemical weapons race, American scientists acquired the ability to synthesize VX in 1958 and continued the development and synthesis of the V series agents (Figure 1). Soviet scientists created the 3rd generation OP "Novichock agents" in the mid 1990's. This was done to evade the current NATO detection and protection measures.

This dissertation follows the style of *Biochemistry*.

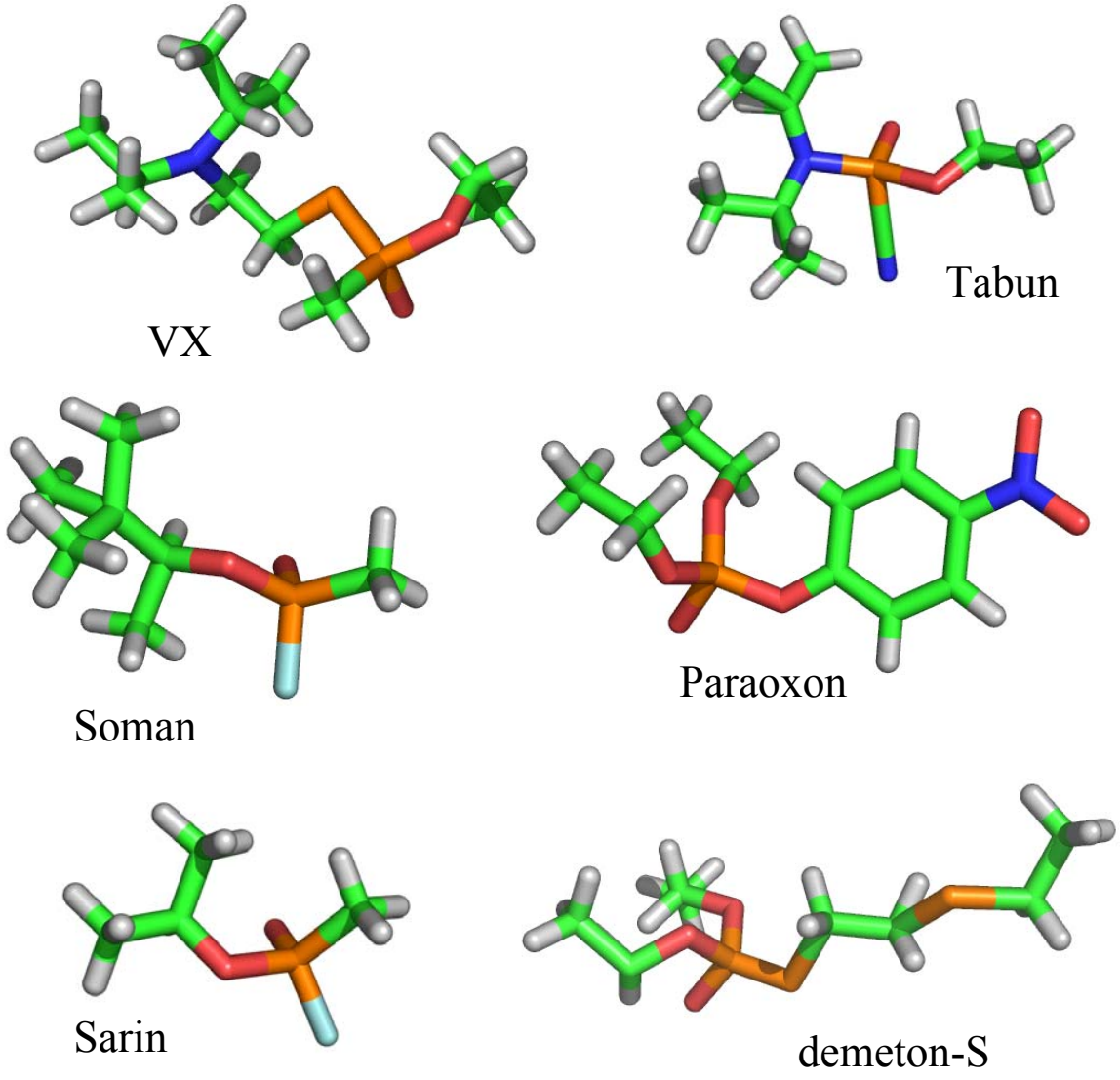

Figure 1: Structures of various organophosphorus compounds.

Of the varying classes of organophosphorus agents, the V series have a neurotoxicity that is 100 fold greater than the G series (Table 1). While the more volatile G agents readily dissipate in the environment, the physical properties of the V series allow them to persist as active agents coating surfaces with an oily film. This makes VX most useful as a "weapon of denial", prohibiting the enemy access to and the use of contaminated space and equipment. Although the use of these weapons is banned by treaties ratified by over 175 nations (particularly the Chemical Weapons Convention of 1997), their physiological and psychological effectiveness continue to make them attractive for terrorist attacks as well as use by rouge nations. The use of CWA (mustard and G agents) against civilians in Iraq during the 1980's and the 1995 sarin attacks in Japanese suburbs and subways in 1993 and 1994 demonstrated the ongoing need for continued vigilance for detection and remediation.

The acute effects of OP neurotoxins exposure are caused by the inhibition of the hydrolysis of acetylcholine to choline by acetylcholinesterase. The build up of neurotransmitters in the synapse produces effects ranging from headaches and dizziness to convulsions and death. In addition to these acute neurotoxic effects, many OP compounds (e.g. leptophos, mipafox, methamediphos, and dichlorovos) can have latent effects, such as organophosphate-induced, delayed-onset polyneuropathy (OPIDPN) (5-7). The proliferation, toxicity, and availability of V-agents make them important targets for detection and decontamination, especially as the world's political climate continues to change. Research into the management of CWA and related agricultural pesticides

Table 1: Relative toxicity based on a 70 kg person and volatility of nerve agents.

Agent	LCt50 (μg·min/m^3)	LD50 (μg)	Volatility μg/m^3 at 77ºF (25ºC)
Tabun (GA)	400	1000	490
Sarin (GB)	100	1700	22,000
Soman (GD)	50	100	3,900
VX	10	10	10.5

benefits the public as well as the military and government agencies, but directly translates into agricultural exposure to neurotoxic poisons.

History of detection and decontamination options for CWA

A timeline of chemical weapon development, decontamination, and protection technologies highlights the historical emphasis on development over protection (Table 2). In the early 1900's CWAs were primarily industrial chemicals, such as chlorine and phosgene that were widely available. During WWI soldiers were equipped with chemical protective masks and coats. The improvements in rubber and synthetic materials through WWII allowed for enhancements in basic protective equipment; however, the development of CWA and more sophisticated delivery systems since WWII has out-paced the effectiveness of the protective equipment. The protective equipment has evolved into better masks with agent specific filters and multilayered over-garments that can absorb and trap toxic chemicals. However, these are just barriers, and do not actively neutralize toxic compounds. A 1997 Government Accounting Office report to the Chairman of the House Subcommittee on Readiness specified the inadequacies of current protective measures (masks and chemical suits) and that the DOD was not prepared for chemical warfare (8). Approved decontamination solutions still largely consist of bleach, which was the decontamination technology of 1914. Barrier protection and caustic decontamination measures are the only deployable systems in use today. Clearly protective measures have not kept pace. Aside from barrier, there are no protective measures available for pre-exposure prophylaxis.

Table 2: Timeline of CW development.

	Agents	***Dissemination***	***Protection***	***Detection***
1900s	Chlorine Chloropicrin Phosgene Mustard gas	Wind dispersal		Smell
1910s	Lewisite	Chemical shells	Gas mask Rosin oil clothing	
1920s		Projectiles w/ central bursters	CC-2 clothing	
1930s	G-series nerve agents	Aircraft bombs		Blister agent detectors Color change paper
1940s		Missile warheads Spray tanks	Protective ointment (mustard) Collective protection	
1950s				
1960s	V-series nerve agents		Gas mask w/ water supply	Nerve gas alarm
1970s				
1980s		Binary munitions	Improved gas masks (protection, fit, comfort)	Laser detection
1990s	Novichok nerve agents			

Atropine/monoxime injectors are currently issued as treatment for post exposure. These anticholinergic compounds have detrimental effects, however, causing restlessness, irritability, hallucinations and the saturation of cholinergic receptors (9,10)

Enzymes: alternatives to caustic decontamination processes

Biotechnologies capable of circumventing the limitations and problems of our present protective measures will require a departure from the current opinion that proteins are fragile biological molecules operational under a narrow range of conditions. Enzymes are involved in many industrial applications. Biotechnological applications have been successful with lipases for the synthesis of biopolymers and biodiesel fuels, as well as the production of enantiomerically pure pharmaceuticals and bulk agrochemicals (11). Furthermore, biocatalytic degradation of pollutants such as chlorinated aliphatic and aromatic compounds has been reported for the decontamination of ground water, soils and aerosols (12). Enzymes are increasingly used in industrial processes, such laccases in stonewashing jeans and agricultural uses such as phytases in feed supplements aiding in the absorption of phosphorus (13).

As our understanding of protein structure and function expands, so will the applications of enzymes. This is particularly true for nerve agent degradation and detection. In addition, the ligand specific interaction of CWA-hydrolyzing enzymes with neurotoxic substrates makes them attractive components in chemical detectors and bio-sensors. The hydrolysis of these highly neurotoxic compounds makes the enzymes invaluable for decontamination and protection without the use of caustic compounds.

Concentrated solutions can be hydrolyzed with base, but the products of the V agents can be as toxic as the parent compounds (Table 3, Figure 2) (14,15). Enzymatic hydrolysis prevents the formation of super toxic compounds such as EA2129 (see Figure 2) by the stereochemical nature of the mechanism involved in the enzyme-substrate complex.

OP degrading enzymes

The best studied pathway for neurotoxic degradation involves a series of *Escherichia coli* genes which code for C-P lyases (carbamate degradation) are located in a 10.9 kb operon consisting of 14 cistrons. These enzymes are capable of hydrolyzing the carbon-phosphorus bond in phosphonates. The enzymatic products of this operon have been well studied in the degradation of environmental contaminants such as the herbicide glyphosate, the antibiotic alaphospholine, and polyaminopolyphosphonic acids used as corrosion inhibitors (16). The intricate regulation and cooperation of the various genes and the proteins, some of which are membrane associated, do not easily lend themselves to CWA applications (17).

Several individual enzymes are capable of hydrolyzing varying chemical bonds found in the OP neurotoxins (P-O, P-S, P-F, and P-CN) (Table 4). Members of this family of enzymes are classified as organophosphorus acid anhydrolases (EC 3.1.8) and are found in species ranging from bacteria to mammals (18-20). Organophosphorus acid anhydrolase (OPAA EC 3.1.8.2) from *Altermonas* sp. is an effective enzyme for the hydrolysis of the P-F bond in soman and can also hydrolyze phosphotriesters such as

Table 3: VX Hydrolysis products from industrial degradation. (Mitretek Systems)

Compound	MW	Solubility, g L^{-1}
EA2192	239.32	-
Methylphosphonic acid, ethyl ester	124.08	-
Diisopropylaminoethanethiol	161.31	-
Methylphosphonothioic acid, ethyl ester	140.14	-
Diisopropylaminoethanol	145.25	78.6
Methylphosphonic acid	96.02	"very"

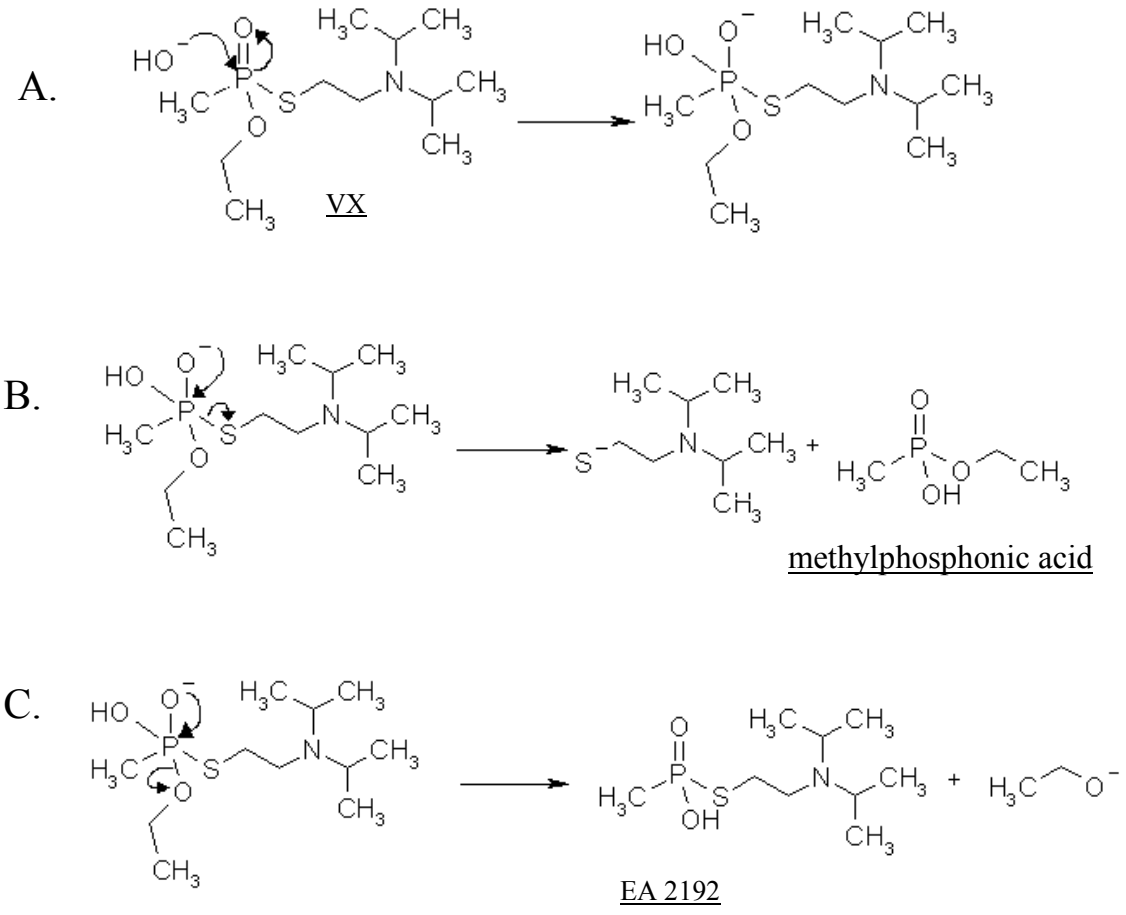

Figure 2: Base hydrolysis of VX showing the production of EA2192.

The first step in the basic hydrolysis of VX is attack of hydroxide on the phosphorus to form a pentacoordinate phosphorus intermediate, panel A. The pentacoordinate phosphorus intermediate can then decompose in one of two ways. In the first mode, the anion of diisopropylaminoethanethiol is expelled to give the ethyl ester of methylphosphonic acid, panel B. In the second, ethoxide is expelled to give EA2192, panel C. (Mitretek Systems)

Table 4: Bonds hydrolyzed by OP degrading enzymes.

	P-O	P-F	P-S	P-CN
OPH	+	+	+	+
OPAA	+	+	-	+
Human PON1	+	+	-	+
Squid DFPase	-	+	-	-

paraoxon, though much less efficiently (21-23). The enzyme is limited by its narrow substrate range and there is little structural and mechanistic characterization. The six fold β-propeller DFPase from the squid, *Loligo vulgaris*, has been studied structurally, but it only hydrolyzes the P-F bond of diisopropyl-fluorophosphate (DFP) (Figure 3A) (24,25).

The serum paraoxonase PON1 (EC 3.1.8.2) also has a six-fold β-propeller structure (26) capable of hydrolyzing a broad spectrum of OP insecticides and CWA (27,28) (Figure 3B). PON1 is an HDL associated metalloenzyme that exists in two allelic forms (A and B) in humans with varying rates of hydrolysis of diazoxon; homozygous type A has a 10 fold higher protection level against diazoxon over the B homozygotes (29). The lack of availability of PON1 for thorough biochemical analysis precludes its use in detection and decontamination applications. Currently, PON1 is purified from serum and cell culture supernatants (30). An overexpression system for PON1 will likely move to the forefront of CWA research because of its presumed immunological compatibility in humans.

Organophosphorus hydrolase (OPH, EC 3.1.8.1) is the most thoroughly studied and best characterized enzyme in the OPAA family. The *opd* gene coding for OPH was isolated from *Pseudomonas diminuta* and *Flavobacterium* sp. in the late 1980's (31,32). OPH is a distorted 72 kD α-β homodimer with one bimetallic active site per subunit (Figure 3C, D). The active site metals are bridged by a catalytic water or hydroxyl moiety, that hydrolyzes substrates via a S_N2 reaction (33). The enzyme catalyzes the hydrolysis of a wide variety of OP compounds containing P-O, P-S, P-F and P-CN

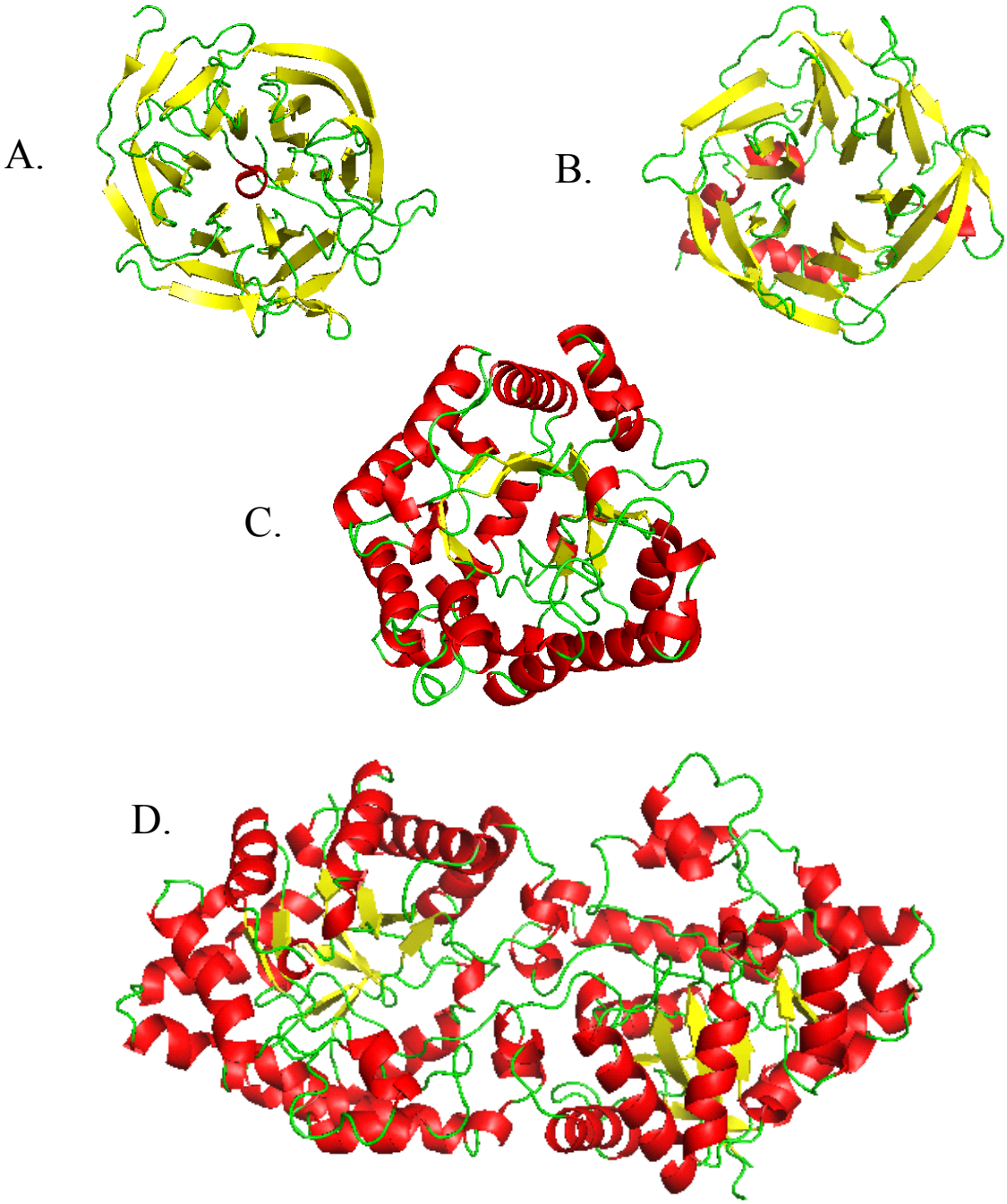

Figure 3: Enzyme structures of the OPAA family. A) DFPase, B) PON, C) OPH monomer, D) OPH homodimer. DFPase and PON are six fold β-propellers and OPH is an α-β protein.

bonds with varying capabilities (Table 4). The enzyme's natural substrate is unknown, yet the hydrolysis of the P-O bond in the phosphotriester insecticide paraoxon appraoches the limits of diffusion (kcat = 6900 s^{-1}) with an efficiency of $1.3x10^{8}$ $M^{-1}s^{-1}$. The activity of OPH as a phosphonothioate (P-S) hydrolyzing enzyme is 1725-fold lower (kcat = 4 s^{-1}) with the pesticide demeton-S (34). The CWA VX (O-ethyl S-diisopropylaminomethyl methlphosphonothioate) and VR (O-isobutyl S (N,N-diethylaminoethyl) methylphosphonothioate) belong to this class of compounds, and the rational design of OPH to enhance the degradation of these poorly hydrolyzed nerve agents is of great interest. The broad substrate spectrum, combined with the existing knowledge about the structure and mechanism of OPH, make it the most attractive enzyme for detection and decontamination applications.

Metals and stability

Metals significantly affect the stability and folding of proteins and half of all proteins in the protein data bank (PDB) are metalloproteins (35). A study examining the effect of transition metals on the dimerization of OXO-10 β-Lactamases from *Pseudomonas aeruginosa* found that melting temperatures could naturally vary as much as 21 ºC with the liganded metal (36). Magnesium binding to alkaline phosphatase was found to linearly correlate with slow changes in protein lability when denatured with guanidinium chloride (GdmCl). Stability was enhanced by higher metal concentrations (37). Most metalloenzymes are very specific in the coordination of metal ions, which can be difficult to replace (38). OPH is unique because it can accommodate and remain

active with many different divalent transition metals (Mn^{2+}, Fe^{2+}, Co^{2+}, Ni^{2+}, Cu^{2+}, Zn^{2+} and Cd^{2+}). Extensive studies have detailed the catalytic properties associated with various metals in OPH, but their effect on stability has not been examined (39,40). The Zn^{2+} form of OPH is among the most stable dimeric proteins known with a ΔG_T of 40 kcal·mol^{-1} (41). OPH unfolds through a three state pathway ($N_2 \rightarrow I_2 \rightarrow 2U$), where the native dimer (N_2) unfolds to an inactive dimeric intermediate (I_2) and finally 2 unfolded monomers (2U). A protein with a similar folding pathway, anticoagualtion factor II (ACFII) from *Agkistrodon actus,* has been studied by GdmCl induced unfolding (42). ACF II has been shown to unfold via a three state pathway similar to that of OPH. Using rare earth metals (Nd^{3+}, Sm^{3+}, Eu^{3+} and Gd^{3+}), reconstituted forms of ACFII were observed to have markedly reduced conformational stability from the native Ca^{2+} form. The stability exhibited linear dependence on the size of the metal ion, with a ΔG_T of 6.7-6.9 kcal·mol^{-1}, fully 6-fold less than that of OPH.

Rational design vs. directed evolution

There are two approaches to the design of enzymes, both capable of generating novel catalytic functions and protein characteristics. Rational design requires structural and mechanistic information for making knowledge-based choices for mutagenesis. This approach has been used successfully to modify a variety of biocatalysts. Site-directed mutagensis has been used to confer catalytic activity on human butyrylcholinesterase (BChE) (43) and to modify or expand the substrate range of OPH (34,42,44,45) Through rational design, toxicity to the mosquito *Culex pipiens* was

introduced by selected deletions and substitutions of the loop residues of domain II *Bacillus thuringiensis* crystal protein Cry1Aa (46). A thermostable lactate oxidase variant was designed to strengthen the interaction between the subunits and stabilize the quaternary structure. This study used a model built on a homologous protein in the absence of a crystal structure (47).

Alternatively, directed evolution of proteins requires a highly selective screen or selection process to detect desirable modifications leading to some preferred function in the target protein. This approach typically involves the random generation of genetic variants by techniques such as regional, site directed mutagenesis or gene shuffling followed by a selection or high throughput screen. This technique has been employed for the development of thermostable enzymes for industrial processes, as well as altered stability, increased pH and organic tolerances (48-52). A combination of both methods has been successful in improving the thermal stability of a 3-isopropylmalate dehydrogenase variant from *Bacillus subtilis*, which was obtained by a triple mutation using site directed mutagenesis followed by PCR based random mutagenesis. The PCR based mutagenesis identified two further stabilizing point-mutations, which were then combined using site directed mutagenesis (53).

Proteins such as OPH benefit from the availability of crystal structures and detailed mechanistic studies. Rational design makes it possible to more precisely tailor the enzyme for a specific application (34,45). This premise was emphasized by subsequent directed evolution studies designed to enhance the hydrolysis of V agents (45,54,55). These “optimized” variants had previously been created using a rational

design approach (45). Finally, rational design is the only method available for adaptation of enzymes for applications which require non-catalytic changes for surface attachment. The development of a screen or selection for this type of application is impractical, because pure enzyme must be used to evaluate the nature of the protein sensing surface.

Rational design of enzymes for sensor surfaces

Enzymes provide both specificity and sensitivity by virtue of their substrate binding interactions. OPH is an enzyme capable of degrading a wide array of OP pesticides and nerve agents (34,56-61) making it ideal for many detection and decontamination purposes.

Several approaches are available for the immobilization of enzymes; the simplest technology is the entrapment in a polymer matrix. OPH has been successfully used to decontaminate surfaces when incorporated in fire fighting foams and latex paints (62,63). This strategy circumvents the many problems caused by the commonly used decontaminating agents such as caustic chemicals. Slightly more complicated, yet still requiring no modification of the enzyme, is the complete encapsulation of enzymes. For example, OPH encapsulation in murine erythrocytes by hypotonic dialysis protected mice against OP pesticide toxicity (64). A sensor based on optical responses utilizing polyethylene glycol (PEG) hydrogel encapsulated OPH was able to detect paraoxon down to 16 nM (0.004 ppm) using pH sensitive seminapthofluorescein (SNAFL) (65).

It has been possible to cryoimmobilize *E. coli* cells expressing OPH to detect paraoxon down to 1.0 μM (0.25 ppm) using a potentiometer biosensor (66).

Slightly more sophisticated non-covalent methods of immobilizing OPH, include examples such as self-assembled chitosan/poly(thiophene-3-acetic acid) layers for the detection of paraoxon down to 1.0 nM (67). It has been possible to detect concentrations of 0.028 nM (7 ppt) paraoxon using OPH-cellulose binding domain fusions, which retained kinetic characteristics similar to the free enzyme when immobilized (68).

Entrapment and non-covalent attachment offer ease of construction; however, the ideal surface would be durable and reusable. Covalent attachment relies on chemical modification of amino acid side chains exposed at the enzyme's surface. Surface attachment through a cystamine-glutaraldehyde linkage was used in developing an amperometric detection system (69), relying on pH change as a result of the release of protons during hydrolysis. OPH has been immobilized in photosensitive polyethylene glycol (PEG) gels, using both covalent attachment and physical entrapment (70). The reversible inhibition of OPH has been utilized for the development of an optical sensor that detects substrate binding rather than the hydrolysis of target compounds (71). In this system, purified enzyme saturated with a porphyrin is immobilized on a glass surface through glutaraldehyde activation of lysines. Therefore, the introduction of a substrate results in the competitive displacement of the porphyrin bound in the active site and the resulting change in the porphyrin absorption spectrum can be observed.

Research study objectives

The objectives of this study were 1) to design a OPH variants with improved stability and adequate catalytic efficiency against OP compounds and 2) to design other OPH variants that, when covalently attached, would improve the efficiency, sensitivity, and reproducibility of a sensor surface.

An evaluation of the available crystal structures of OPH reveals a stacking network among the three dimensional orientations of residues 254 and 257 with respect to the active site and neighboring residues (56,72). In the present study, the role of aromatic stacking and cation-π interactions involving these residues in establishing the stability of the enzyme is investigated. Monitoring changes in fluorescence emission by excitation of tyrosinyl and tryptophanyl residues, as well as circular dichroism (CD), has allowed measurement of changes in the global conformation of OPH. The selective excitation of tryptophan residues, and their close proximity to residues 254 and 257, has allowed the observation of local changes in the protein. This study provides insight into the integration of structure and function in OPH, leading to the design and construction of OPH enzymes that balance activity and stability.

Furthermore, enzyme immobilization strategies are quite varied; each has advantages and disadvantages that will likely preclude the use of a single technique. An extensive review has been published by Russell et al. that details not only OPH, but other enzymes in biomaterials for detection and decontamination of chemical warfare agents (73). The issues of efficiency and reproducibility in enzyme attachment to reactive surfaces are addressed in this study, presenting a method to further refine

orientation by the construction of a surface orientation-specific OPH variant. Ideally, this kind of attachment should facilitate movement of substrates and products to and from the active sites, as well as stabilize secondary structure against chemical and thermal denaturation.

MATERIALS AND METHODS

Variant construction and mutagenesis

The RH, RL, and HL variants were created in the leaderless (Δ 2-29) wild type *opd* gene cloned into pUC19 (39) as previously described (45). The two digit nomenclature refers to position 254 and 257, i.e. the wild type HH has a histidine at both position 254 and 257. The leucine at position 257 in the RL variant was replaced with a phenylalanine to generate the RF variant using the QuikChange XL mutagenesis kit (Stratagene). Primers to construct the L257F mutation were 5'-gcatcccgttcagtgcgattggtctag-3' and 5'-ctagaccaatcgcactgaacgggatg-3'. Primers to construct the K175 variant were 5'-aaaggggtcgcgcagcctgtggtc-3', 5'-gaccacaggctgcgcgacccccttttca-3'. All primers were synthesized by Integrated DNA Technologies (IDT). The putative plasmids were transformed into *E. coli* DH5α for replication and purification. All variants were sequenced to confirm the presence of the mutation and verify the integrity of the gene.

DNA sequencing

Two μl Big-Dye^{TM} Terminator Mix (PE Applied Biosystems), 3.2 pmol primer (5'-ttgtcgatactggtactaat-3') , and 100 ng plasmid DNA were brought to 7.0 μl with DI H_2O. The sequencing cycle consisted of an initial denaturation of 5 min at 95 °C, followed by 25 cycles of 95 °C for 30 s, 50 ºC for 30 s, and 60 ºC for 4 min. A final elongation at 60 ºC is done for 10 min and the reaction held at 4 ºC. Unincorporated

nucleotides were removed with Bio-Rad P-30 Micro Bio-Spin Columns. The spin columns were inverted to resuspend the matrix material and the buffer centrifuged into a collection tube. The matrix material was washed 3X with H_2O by centrifugation at 1000 xg, followed by a final spin to dry the matrix material. The wash was discarded. The sequencing reactions were adjusted to 20 µl and carefully added to the center of the matrix column, then centrifuged at 1000 xg for one min into a collection tube. The reactions were dried under vacuum and sent to GTL (Gene Technologies Laboratory, Texas A&M University) for analysis. Sequenced plasmids were transformed into *E. coli* DH5α for protein expression and enzyme purification.

Plasmid mini-prep

Isolated colonies from the transformations were grown in 5 ml L-Broth at 37 ºC overnight and plasmid mini preps were used for sequencing. One and a half ml of culture was transferred to a micro centrifuge tube, centrifuged for 2 minutes and the supernatant decanted. The bacterial pellet was resuspended in 100 µl of cold GTE (50 mM glucose, 25 mM Tris-Cl, pH 8.0, 10 mM EDTA, pH 8.0) by vortex mixing. Two hundred µl of freshly prepared NaOH/SDS (1 ml 10% SDS, 0.4 ml 5 M NaOH, 8.6 ml DI H_2O) was added and the tube inverted several times. Finally, 150 µl of cold KOAc (60 ml 5 M potassium acetate, 11.5 ml glacial acetic acid, 28.5 ml DI H_2O) was added and the tube gently inverted 3-5 times, and incubated on ice for 5 minutes. Following centrifugation for 5 minutes, the supernatant was transferred to new tube. Two volumes of absolute ethanol were added and the tube inverted several times and incubated at -20 ºC for 1 hr.

The nucleic acids were pelleted by centrifugation at 10,000 xg for 2 min. The pellet was washed with 70% ethanol, centrifuged for 2 minutes and the supernatant decanted. The pellet was dried under vacuum and resuspended in 10 µl H_2O and stored at -20 ºC.

DH5α transformation

Competent cells were prepared by inoculating 5.0 ml of L-Broth with a single colony and shaking over night at 37 °C. The bacteria were resuspended and mixed 1:1 with TSB (10 % PEG (MW=3350), 5 % DMSO, 20 mM $MgCl_2$, 20 mM glucose in L-Broth), dispensed in 50 µl aliquots and stored at -80 ºC. Bacteria transformed with pOP419-WT or pOP419-257L were plated on LB (10 g bacto-tryptone, 5 g bacto-yeast extract, 10 g NaCl , 15 g agar, dissolved in 1.0 L water, adjusted to pH 7.0 and autoclaved) plates containing 50 µg/ml ampicillin (amp) and incubated overnight at 37 ºC. A single colony from each transformation was used to inoculate 5.0 ml LB^{amp} medium and incubated with shaking at 37 ºC overnight. Ten ml of overnight culture was used to inoculate 1.0 L terrific broth (TB, Difco) supplemented with 0.4% glycerol, 50 µg/ml ampicillin, 1.0 mM $CoCl_2$, which was incubated at 30 ºC for 40 hr with shaking and the cells harvested by centrifugation at 4000X g.

Enzyme purification

The enzymes were purified as previously described (41). Purified enzymes were concentrated to greater than 1 mg/ml for storage at 4 °C in the final column buffer (10 mM KPO_4, 20 mM KCl, 50 µM $CoCl_2$, pH 8.3). Protein concentrations were determined

by using an extinction coefficient of 58,000 $M^{-1}cm^{-1}$ at 280 nm. Purity was verified by SDS-PAGE with coomasie blue staining.

Metal chelation and reconstitution

Purified enzyme was dialyzed against 2.0 mM, 1,10 phenanthroline in phosphate buffer (10 mM KPO_4, 20 mM KCl, 50 μM CoCl, pH 8.3) until the activity was less than 1% of the initial activity with paraoxon. The phenanthroline was removed by extensive dialysis in phosphate buffer. Enzymes were reactivated by dialyzing in phosphate buffer containing 10 mM bicarbonate and 10 mol equivalent metal (Mn^{2+}, Co^{2+} or Zn^{2+}) (40).

Equilibrium chemical denaturation

Chemical denaturation experiments were done as previously described (41,72). The final concentration of enzyme was 100 μg/ml for all denaturation experiments. CD and fluorescence samples were incubated for 24 hr at 25 °C in 0-4 M GdmCl or 0-8.5 M urea. Denaturants were prepared in 10 mM phosphate 50 μM $CoCl_2$, 20 mM KCl buffer, pH 8.3 (74). CD spectra were collected on an AVIV 202, with an averaging time of 30 s at 25 °C in 0.5 cm path length cuvettes. Fluorescence data was collected on an AVIV 105ATF fluorometer using an excitation wavelength of 278 nm and the emission recorded at 320 nm, with a signal averaging time of 30 s at 25 °C with 1 cm path length cuvettes.

Fluorescence signals were normalized to represent the fraction folded (f_F) using equation 1, where Y_{Min} and Y_{Max} are the minimum and maximum fluorescence intensities, and x is the intensity at any given denaturant concentration.

Eq. 1. $$f_F = \frac{Y_{Min} - x}{Y_{Min} - Y_{Max}}$$

By use of the relationship $f_F + f_I + f_U = 1$, where $f_F = [N_2]/[P]_T$, $f_I = [I_2]/[P]_T$ and $f_U = [U]/[P]_T$, the fraction in the native state, intermediate and unfolded states were used to solve for K_1 and K_2, where $K_1 = f_I / f_N$ and $K_2 = [P]_T f_U^2 / f_I$, where $[P]_T$ = total protein, f_I = the fraction in the intermediate state, and f_U = the fraction in the unfolded state. The equilibrium constants were fit to equation 2 using the nonlinear least squares fitting tool in Origin 7 to calculate the total Gibb's free energy of folding (ΔG_T) for a 3 state model.

Eq. 2. $$\Delta G_T = -RT \ln K_1 + RT \ln K_2$$

Thermal denaturation

Fluorescence data for thermal denaturation were collected on an AVIV 105ATF fluorometer using an excitation wavelength of 278 nm and the emission recorded at 320 nm with a signal averaging time of 30 s in sealed 1cm path length cuvettes. The protein

was equilibrated for 15 min at each temperature step with fluorescence spectra collected from 25-85 °C. Apparent melting temperatures were calculated by fitting the data to equation 3, where $\Delta G = 0$ and $\Delta H = T_{M\,app}\Delta S$.

Eq. 3. $$\Delta G = -RT \ln \frac{f_U}{f_F}$$

The fraction folded was calculated as above in equation 1 where $f_F + f_U = 1$.

Tryptophan excitation

Wave scans for the HH enzyme and each variant were collected with an AVIV 105ATF spectrofluorometer by exciting at 295 nm and recording the emission at 320 nm at 25 °C. Protein concentrations were checked using the extinction coefficient and the Bradford assay to ensure all variants were at 100 µg/ml.

Thermolysin digestion of OPH

Thermolysin digests were done at 65 °C at an OPH:Thermolysin ratio of 250:1 with 5 µM $CaCl_2$ in 10 mM Tris (pH 8.3). OPH was incubated for 2 min at 65 °C, and then the thermolysin was added to initiate digestion. Aliquots were removed at 1, 5 and 15 min. The digestion in the aliquots was stopped by addition of SDS loading dye and boiling for 5 min. Proteolysis samples were then analyzed by SDS PAGE. The relative band intensities between 1 and 15 min, as determined using TotalLab v2005, were fit to

equation 4 to determine the half lives of the enzymes under these conditions, where t_0 is the band intensity at 1 min and $t_{1/2}$ is one half t_0. As with the tryptophan excitation experiments, the protein concentrations were determined using the extinction coefficient and the Bradford assay to ensure all variants were at the same concentration.

Eq. 4. $$[A]_{t_{\frac{1}{2}}} = [A]_{t_0} e^{-kt}$$

Enzyme surface characterization

The PDB file 1DPM was submitted to the Parameter Optimised Surfaces (POPS) at http://ibivu.cs.vu.nl/programs/popswww/, to calculate accessible surface area at the residue level. Percent burial of the ζ-N was performed using *pfis,* which calculates accessible surface area by comparing a residue to a model tripeptide, GXG, giving information at the atomic level.

Enzyme biotinylation

The enzymes WT and K175A (1 mg/ml) were incubated with equal concentrations of Biotin (Pierce, Rockford, IL) in 5% DMSO, 10 mM KPO_4 pH 8.3 overnight on a shaker at 4 ºC. The unbound biotin was removed by dialysis performed overnight in 10 mM KPO_4 (pH 8.3) at 4 ºC. This work was performed in association with Dr. Aleksandr Simonian, Auburn University.

OPH enzymatic activity assay

Paraoxon and demeton-S were purchased from ChemService. The free thiol reporter for the demeton-S assays was 2,2' Dithiodipyridine (2,2' TP)(Sigma) and DTNB (Ellman's reagent)(Sigma) for VX and VR. The CWA VX and VR in saline were provided by ECBC (Edgewood Chemical Biological Center, Aberdeen Proving Ground, Maryland), and assays were performed at the US Army Medical Research Institute of Chemical Defense, Aberdeen Proving Ground, Maryland. Michaelis constants (K_M) and the catalytic rates (k_{cat}) for paraoxon and demeton-S were determined by performing enzymatic assays with varying concentrations of substrate and constant enzyme concentrations. The data were fit using Origin 7.0 software (Microcal).

Paraoxon hydrolysis was followed by measuring the appearance of the p-nitrophenol anion at 400 nm (ε = 17, 000 $M^{-1}cm^{-1}$) in 20 mM CHES (pH 9.0) at 25 °C, and initial velocities were calculated and fit to equation 5, allowing for substrate inhibition.

Eq. 5. $$v_o = \frac{V_{max} \times S}{K_M + (S \times (1 + \frac{S}{K_i}))}$$

Demeton-S hydrolysis was followed by the appearance of the 2,2' TP anion at 343 nm (ε = 7,060 $M^{-1}cm^{-1}$) in Tripart buffer pH 8.0 {di Sioudi, 1999 27 /id} and initial velocities were calculated and fit to equation 6.

Eq. 6. $$v_O = \frac{V_{\max} \times S}{K_M + S}$$

Immobilized enzyme activity

In order to calculate the activity of the immobilized enzyme, 0.05 mM paraoxon was circulated across the surface at a flow rate of 100 µl/min for 2 min. Paraoxon hydrolysis was measured by collecting 200 µl of the effluent at various time points and measuring the absorbance at 405nm to determine the paraoxon remaining. The rate of hydrolysis was determined by calculating the concentration of enzyme on the sensor surface. This work was performed at Auburn University.

Analysis of OPH activity with G agents

Activity with G agents consisted of a linked assay which measured the Butyrylcholinesterase (BuchE) activity remaining after exposure to agent. Serial dilutions of BuchE were prepared and incubated against the available G agent stocks (GA, GB, GD and GF) to determine the concentration just necessary to completely inhibit BuChE. that would be completely inhibited. Once the BuchE concentration for each agent had been determined, that amount of agent was pre-incubated with 10 ng of OPH for 1 hour. After this pre-incubation, BuchE was added to the OPH/agent mixture, allowed to inhibit for 20 minutes and assayed immediately as previously described. Any BuChE activity detected following the agent exposure indicated OPH hydrolysis of the agents. This work was performed at USMARICD, Aberdeen, MD in collaboration with Dr. Douglas Cerasoli.

SPREETA preparation and sensing layer construction

The sensor surface was cleaned with piranha solution (5:1 mixture of H_2SO_4 and H_2O_2) followed by rinsing and sonication with Milli-Q water. The sensor was then initialized in air and water, followed by in-situ cleaning with 0.12 N NaOH,1%Triton X. After establishing a baseline with PBS (0.137 M NaCl, 2.7 mM KCl, 4.3 mM Na_2HPO_4 $7H_2O$, 1.4 mM KH_2PO_4, pH 7.4), neutra-avidin (1 mg/ml) was non-specifically adsorbed on the gold surface. BSA (1 mg/ml) was used to block the remaining sites, followed by specific immobilization of biotinylated enzymes, (WT, K175A) at 1 mg/ml. This work was performed in collaboration with Dr. Aleksandr Simonian at Auburn University.

Calculation of surface coverage

The amount of enzyme covering the surface of the sensor was calculated with equations 7, 8 and 9. First the adsorbed layer (ad-layer) thickness is calculated as

Eq. 7. $$d_a = \left(\frac{l_d}{2}\right) * \left(\frac{n_{eff} - n_b}{n_a - n_b}\right)$$

where d_a = the thickness of the ad-layer, l_d = the characteristic decay length ~ 307nm, n_{eff} = effective RI of the ad-layer (from SPR signal), n_b= RI of the buffer, 1.333, and n_a = RI of the proteins, 1.57. Surface coverage is calculated by the thickness and density of the protein.

Eq. 8. $$\text{Surface coverage}\,(\text{g/mm}^2) = \text{thickness}\,(d_a) * \text{density}\,(\approx 1.3\ \text{g/ml})$$

Eq. 9. $$\text{Surface coverage}\,(\text{molecules/mm}^2) = \frac{\text{Surface coverage}\,(\text{g/mm}^2) * \text{Mol wt.}}{\text{Avagadro's Number}}$$

Antibody binding

The sensor surface was cleaned with "piranha solution" followed by rinsing and sonication with Milli-Q water. The sensor response was then initialized in air and water followed by in-situ cleaning with 0.12 N NaOH,1%Triton X. After establishing a baseline with PBS, neutra-avidin (1 mg/ml) was non-specifically adsorbed on the gold surface. BSA (1 mg/ml) was used to block the remaining sites, followed by specific immobilization of biotinylated enzymes (WT, K175A – 1 mg/ml). Polyclonal antibody (1:100) against OPH was introduced into the flow chambers and the surface coverage of the enzyme-antibody complex was calculated from the measured response units, as described above.

RESULTS

Wild type stability and metals

Apo-OPH was created by dialyzing purified enzyme against 2 mM phenanthroline until the original catalytic activity had been reduced to below 1%, and the phenanthroline was removed by extensive dialysis. The various metal forms of OPH were reconstituted by dialysis of the apo-enzyme against 10 molar equivalents of metal in the presence of bicarbonate. Enzymatic activity of the metal bound enzymes was evaluated by measuring paraoxon hydrolysis. The conformational stabilities were determined from urea induced equilibrium unfolding. The unfolding profile of each enzyme form differs primarily in the $N_2 \rightarrow I_2$ transition (Figure 4). The free energies for folding for the Zn^{2+}, Co^{2+}, and Mn^{2+} enzymes are given in Table 5, with the Zn^{2+} form possessing a ΔG_T unfolding almost twice that of the Co^{2+} or Mn^{2+} bound OPH.

The corresponding activity with paraoxon for each of the metal forms of the enzymes is given in Table 5. Although the Zn^{2+} enzyme is much more stable, the ΔG_T unfolding for the Co^{2+} and Mn^{2+} forms are still higher than other dimeric proteins (41).

Characterization of the native OPH enzyme and 254/257 variants

Four variants of OPH were created by Lai et al. (45), by substituting the native histidines at positions 254 and 257 in OPH. With the exception of a single enzyme, the RH variant (H254R), the Gibb's free energies for folding were determined from the chemical equilibrium denaturation data (Table 6). Comparison of the ΔG_T unfolding

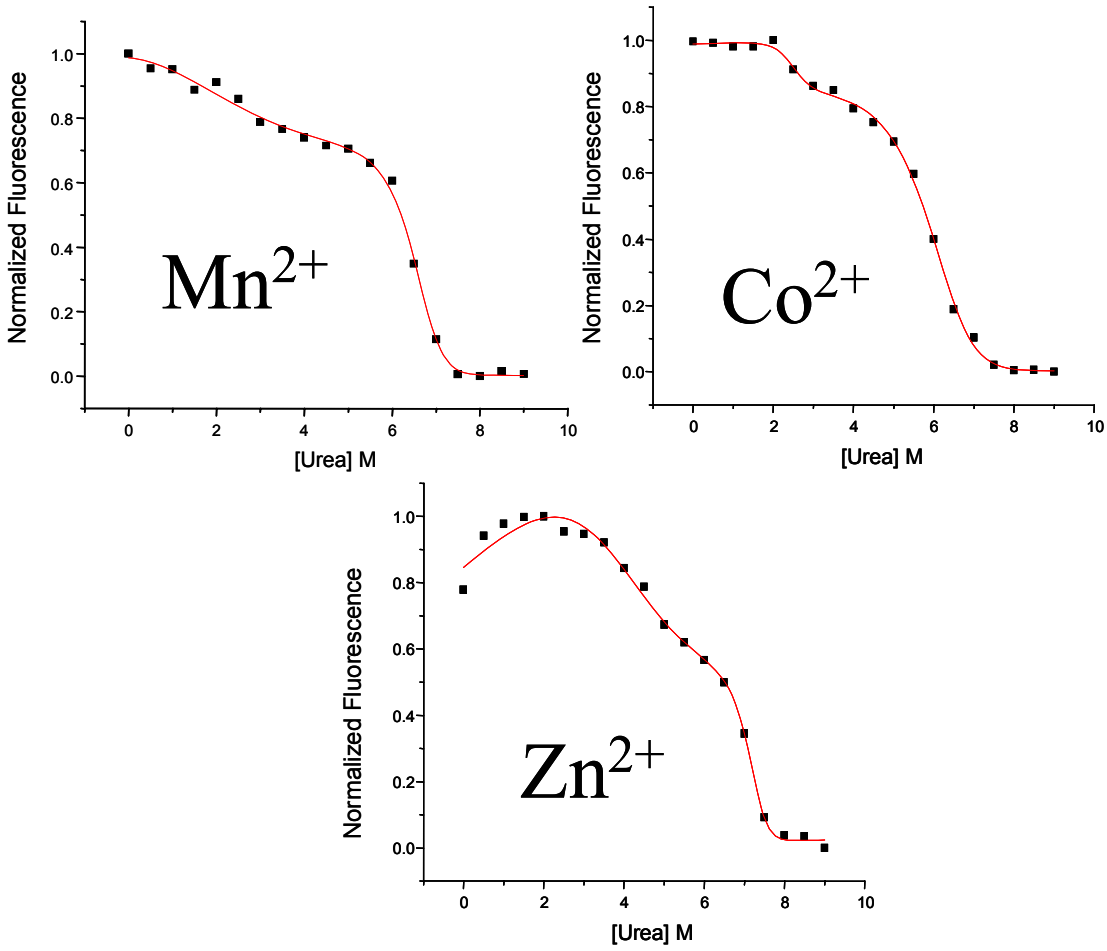

Figure 4: Equilibrium denaturation of the wild type metal forms. The Y axis is the fluorescence emission of each enzyme normalized to the signal intensity in the absence of denaturant. The more stable Zn^{2+} form shows an increase in intensity at low denaturant concentrations indicative of a structural rearrangement of the enzyme. The zinc data is consistent with that previously reported (41).

Table 5: Thermodynamic stability of OPH metal forms. The relative catalytic rates (kcat $\cdot s^{-1}$) paraoxon are given for reference.

Metal	ΔG_T (kcal/mol)	T_{Mapp} (°C)	k_{cat} (s^{-1})
Zn^{2+}	40 ± 3	75.0 ± 0.3	900
Co^{2+}	22 ± 2	71.0 ± 0.2	6700
Mn^{2+}	25 ± 2	67.0 ± 0.3	600

Table 6: Thermodynamic stability of HH, RL and HL variants. Values reported in kcal/mol as determined by equilibrium urea denaturation, followed by intrinsic tryptophan fluorescence.

Enzyme		ΔG_1	ΔG_2	ΔG_T
HH	H254, H257	3.4 ± 1.3	21.9 ± 1.9	25.3 ± 3.2
RL	H254R, H257L	2.3 ± 0.6	17.3 ± 0.9	19.6 ± 1.5
HL	H254, H257L	0.9 ± 1.0	19.4 ± 1.0	20.3 ± 2.0
RH	H254R. H257	ND*	ND*	ND*

* Not Determined

values allowed for an evaluation of each substitution's contribution to the global stability. The denaturation curves revealed that the transition from the native state to the intermediate, $N_2 \leftrightarrow I_2$ in the unfolding pathway, was variable among the HH, RL, and HL enzymes, while the transition from the intermediate to unfolded monomers, $I_2 \leftrightarrow 2U$, was basically uniform (Figure 5). The $N_2 \leftrightarrow I_2$ variability may be due to the close proximity of residues 254 and 257 to W302, which are only 8.4 and 5.1 angstroms, respectively from W302. This would be close enough to produce deviation in the spectra by quenching through energy transfer among the aromatic residues (Figure 6). This may be further complicated by changes in the tertiary structure in the presence of denaturants.

The RH variant, which retained its aromatic histidine at position 257, had complex intrinsic fluorescence spectra between 1 and 2 M GdmCl (Figure 7 A). The spectra in this concentration range possessed two transient inflections prior to the intermediate state, resulting in an inability to fit the data with a three state model. The $I_2 \leftrightarrow 2U$ transition was shifted to 2.5-3 M GdmCl, slightly higher than the 2-2.5 M range of the other variants. In fact, this enzyme was not completely denatured by concentrations up to 8.5 M urea after incubation for 24 hr, as evidenced by the lack of a post-transition in the urea curve (Figure 7 B). This indicated that some fraction of the enzyme remained in the folded form, suggesting the RH variant was a much more stable enzyme than wildtype OPH. This was supported by GdmCl denaturation profiles, which indicated some RH enzyme retained residual activity above 2 M GdmCl (Figure 8). The complex spectra in the pretransition and the incomplete denaturation in the post-transition region of the equilibrium unfolding curves prevented the determination of free

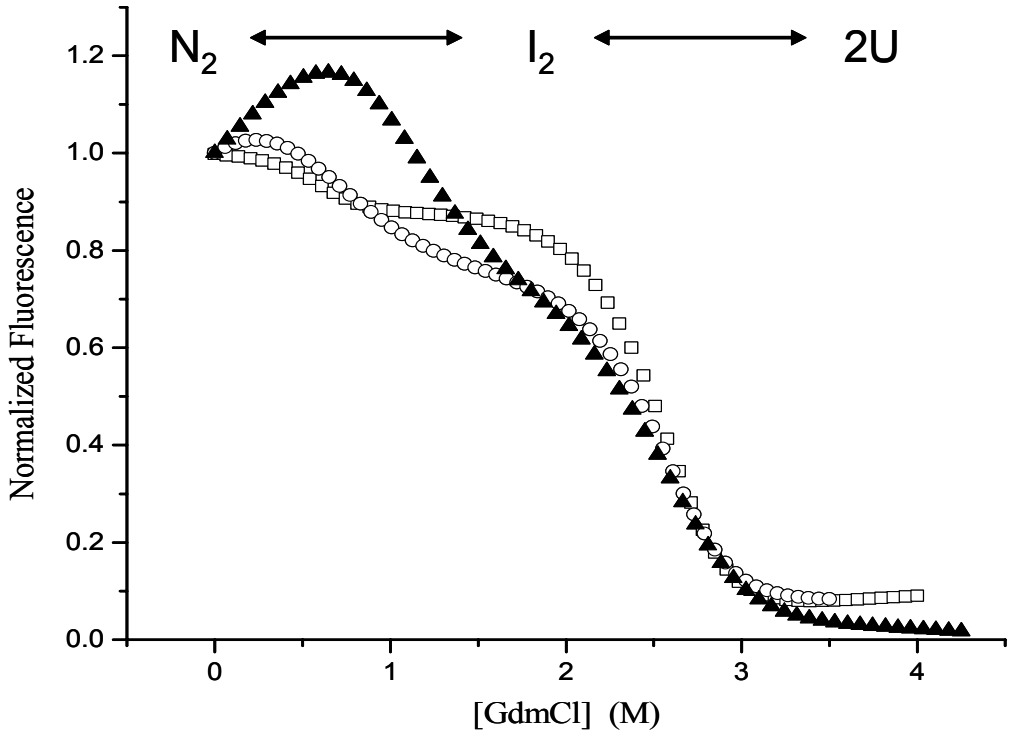

Figure 5: Emission spectra of the WT, RL and L variants showing the variability in the $N_2 \rightarrow I_2$ transition with GdmCl denaturation. WT (open squares), L (closed triangles), RL (open circles). The transition from the native dimer to the inactive dimeric intermediate is not uniform, as is the second transition from the intermediate to the unfolded monomers.

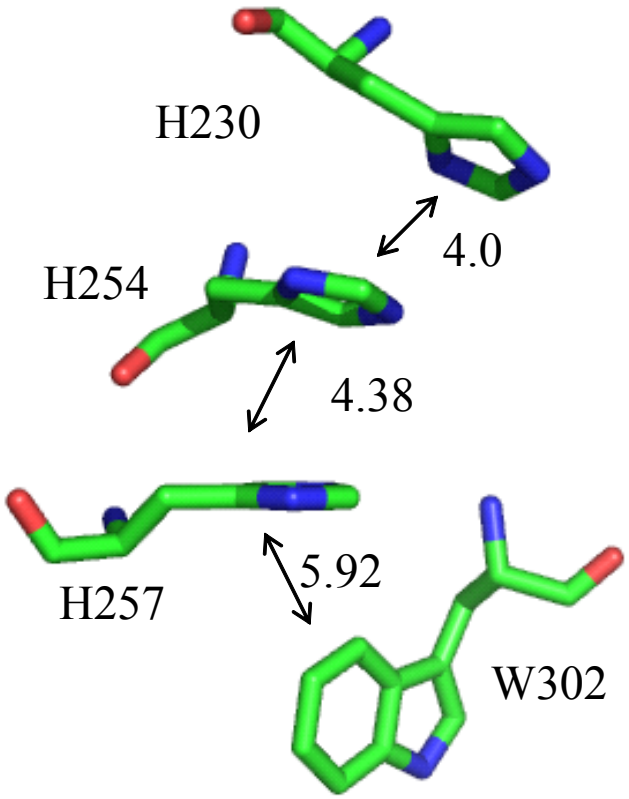

Figure 6: Spatial relationships of H230, H254, H257 and W302. Distance given in angstroms.

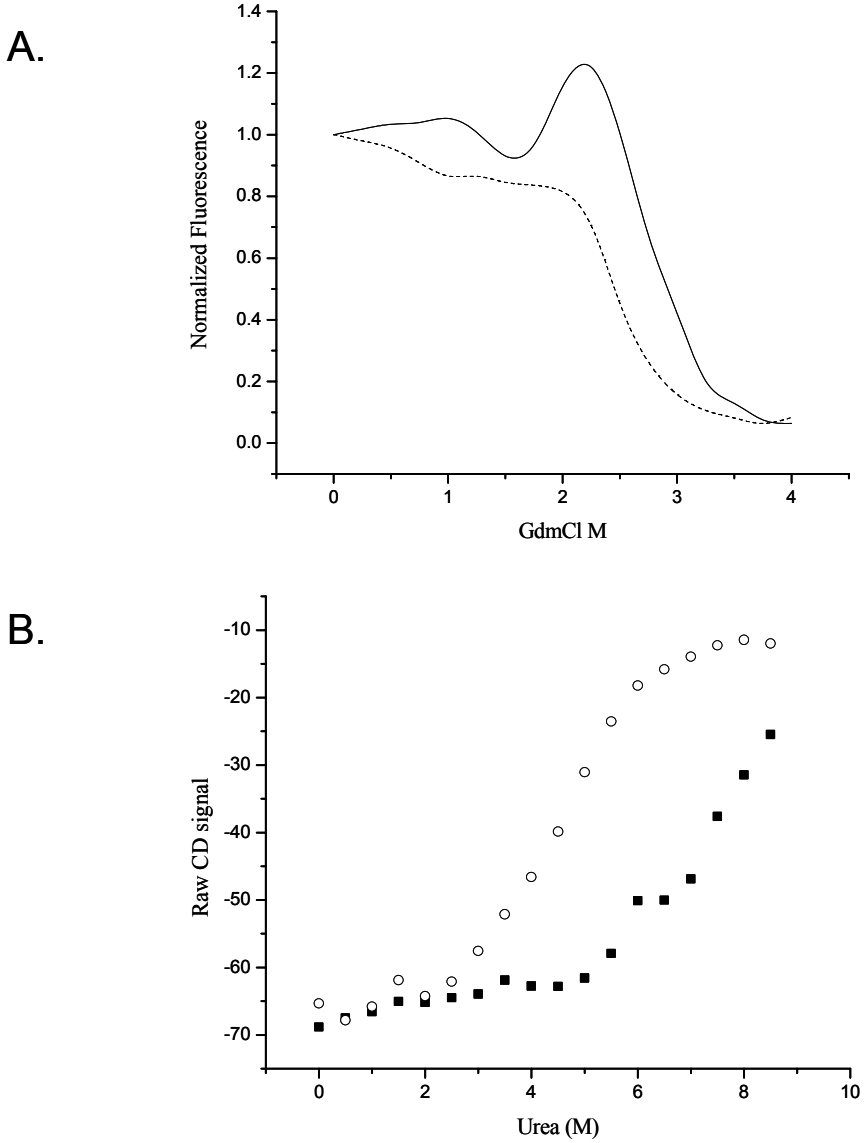

Figure 7: GdmCl and urea denaturation of the HH and RH variants.

A. GdmCl denaturation data of the RH (solid line) followed by intrinsic tryptophan fluorescence. The native HH enzyme, (dashed line), is shown for reference. The RH variant displays complex spectra between 1 and 2.5 M GdmCl indicating structural changes not present in the HH at these denaturant concentrations.

B. Urea denaturation data of the RH (■) and HH (○) followed by CD at 222 nm. RH was not completely denatured even at 8.5 M urea as evident by the lack of a post transition in the denaturation curve.

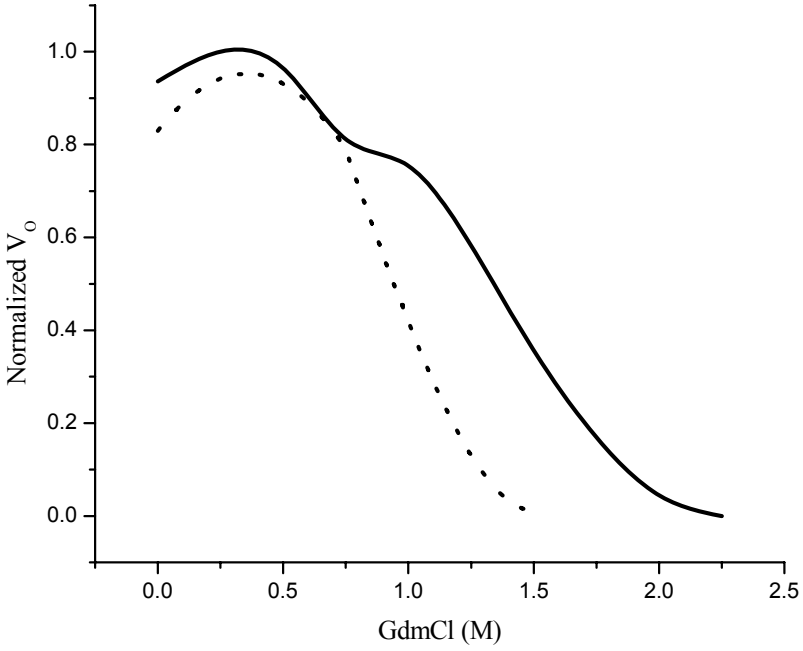

Figure 8: Activity profile during GdmCl inactivation of HH and RH variants. The HH (dotted line) and RH (solid line) enzymes display a similar increase in activity with paraoxon at low denaturant concentrations, however, the RH variant has a distinctive plateau at 1.25 M GdmCl.

energies of folding for the RH variant. The denaturation data of those variants that fit the three state model supported the hypothesis that the substitution of a leucine at position 257 plays an important role in the decreased stability of these enzymes.

Design and characterization of a more stable P-S hydrolyzing enzyme

Variants with an arginine at position 254 have a 10-12 fold increase in activity with P-S substrates (34,39,45,76); however, the most efficient of the P-S hydrolyzing enzymes, RL, is also much less stable than the HH enzyme (Table 7). Evaluation of the HH crystal structure reveals that the orientation of 257 with 302 creates an edge-to-face stacking interaction (Figure 9A) (Benning et al. 1994). Disruption of this interaction, as with the RL and HL variants, leads to less stable enzymes. Thus, engineering a substitution at position 257 to provide a stronger interaction with 302 should result in a more stable enzyme. Combining this substitution with the arginine at position 254 should confer the desirable P-S activity of the H254R variant. To test this hypothesis, the leucine at position 257 in the RL variant was replaced with the more hydrophobic phenylalanine to produce the H254R H257F (RF) variant.

Chemical denaturation curves of the RF variant displayed the same complex spectra during the $N_2 \leftrightarrow I_2$ transition seen with the RH enzyme, so the ΔG_T could not be determined (Figure 10). The fluorescence quenching between 1 and 2 M GdmCl that was observed for the RH and RF variants in the pretransition region might have resulted from denaturation and the corresponding exposure of tryptophan residues to solvent. However, CD spectra over this concentration range showed an initial increase in

Table 7: Enzyme activity comparison of the HH, RF, RH and RL variants.

	Enzyme	Paraoxon		demeton-S		VX	VR
		k_{cat} s^{-1}	K_M mM	k_{cat} s^{-1}	K_M mM	k_{cat} s^{-1}	k_{cat} s^{-1}
HH	H254, H257	6900	0.1 ± 0.05	3.5	6.1 ± 1.7	14	12
RF	H254R H257F	450	0.05 ± 0.02	34	0.05 ± 0.02	68	36
RH	H254R, H257	1200	0.09 ± 0.01	32	6.6 ± 1.0	ND*	ND*
RL	H254R. H257L	640	0.07 ± 0.01	50	8.2 ± 1.4	144	465

* Not Determined

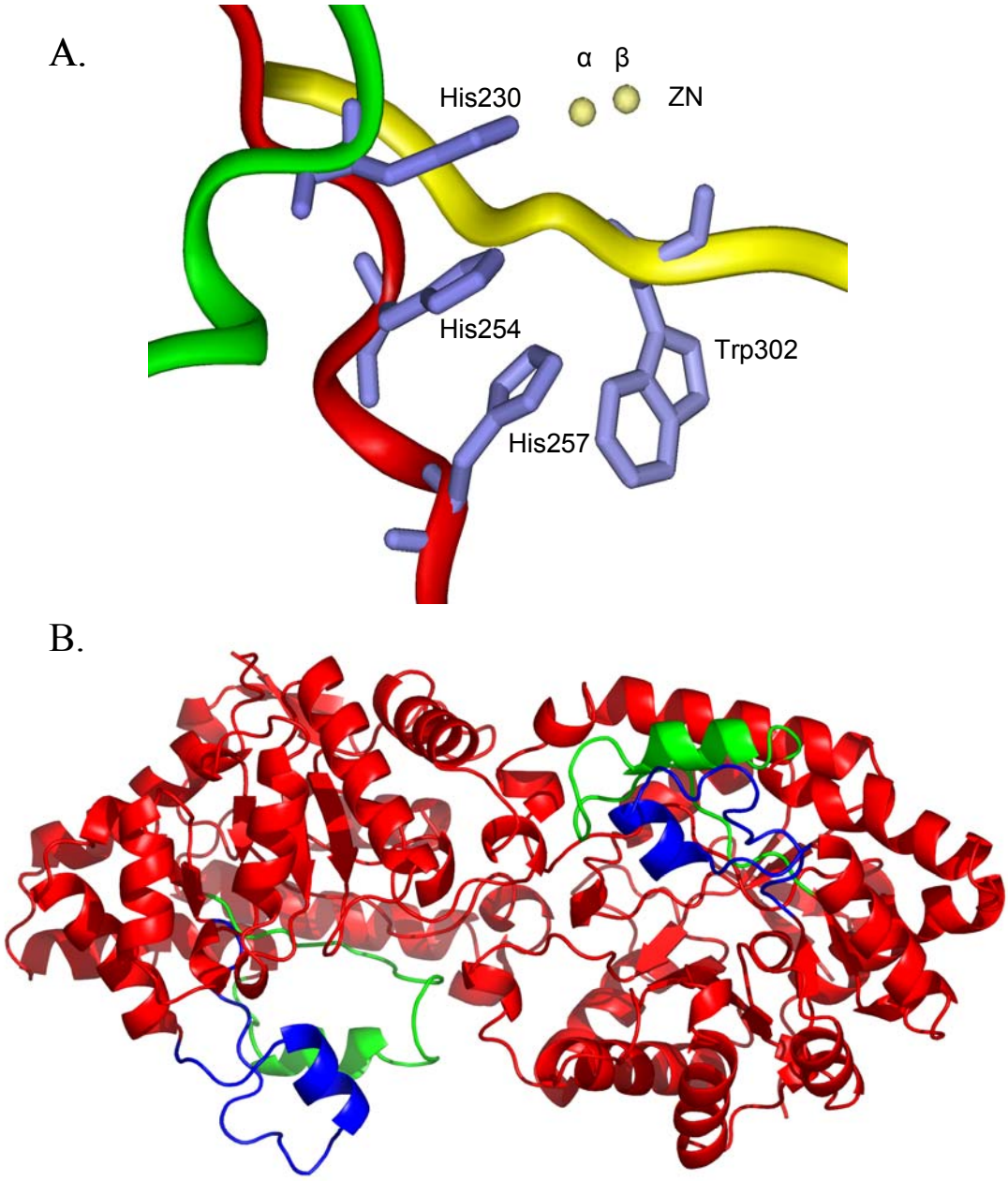

Figure 9: Stacking network and dimer illustration of OPH.

A. The active site metals of OPH and the stacking network consisting of H230, H254, H257 and W302. The green, red and yellow distinguish three secondary structural elements with residues involved in the stacking network

B. Regions adjacent to the opening to the active site are depicted in green (residues 299-323) and blue (residues 253-276).

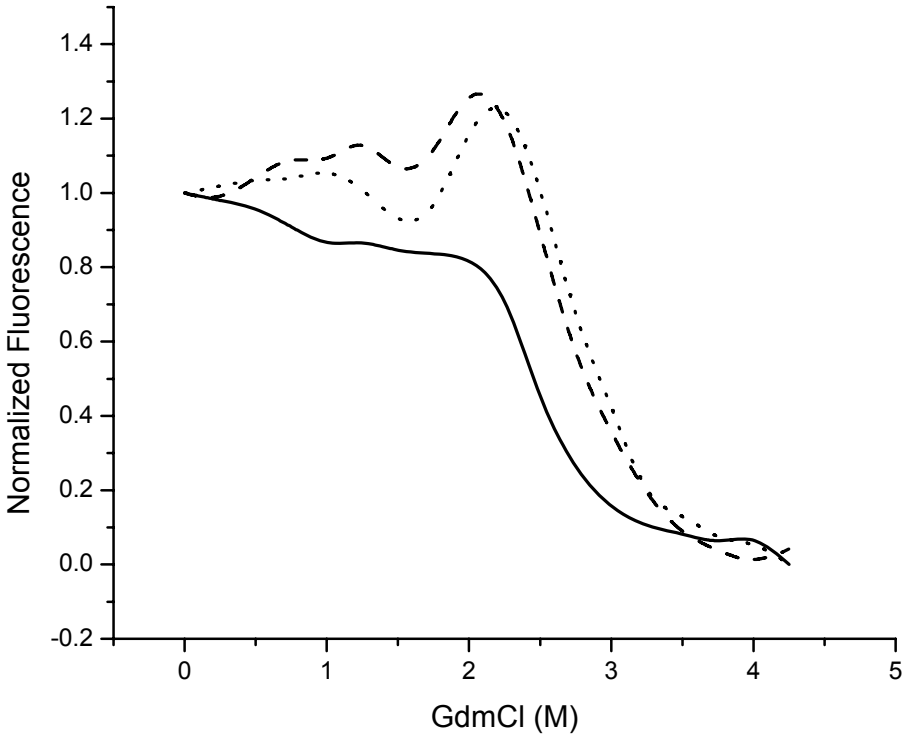

Figure 10: Comparison of GdmCl denaturation profiles of the HH, RH and RF enzymes. Normalized fluorescence of the HH (solid line), RF (dashed line) and RH (dotted line) enzymes. The RH and RF variants display similar local minima at 1.5 M GdmCl not present in the HH enzyme. The RH and RF are also similar in the transition to the unfolded monomers, which is shifted from 2.5 to 3.0 M GdmCl when compared to the HH enzyme.

secondary structure content relative to the native state for the RF and RH. At 222 nm the RH enzyme displayed an increase in the CD signal below 1 M GdmCl, increasing 7% from 0-0.75 M GdmCl, then continually lost signal above 1 M denaturant. The HH enzyme loses signal at all denaturant concentrations (Figure 11). The RF variant displays a plateau in activity at these GdmCl concentrations, indicating a more complex unfolding pathway when compared to the wild type, with possibly two or more intermediates. Together, these data suggest that the movement of one or more neighboring residues in proximity to the fluorophore causes quenching of the fluorescence signal. This quenching could result from either an extension of helices 15 and 18 in the unstructured loops (Figure 9B) and/or a compaction of the overall structure below 1 M GdmCl. The increase in secondary structure at these denaturant concentrations supported the conclusion that the enzyme was not unfolding.

Whereas the ΔG_T of some of these variants could not be determined by chemical denaturation, limited proteolysis during temperature denaturation was used to evaluate the relative stabilities. The paradigm is that compact or folded structures have fewer available proteolysis sites, and they are thus more resistant to degradation (77). The susceptibility of each variant to thermal denaturation was followed by thermolysin digests after 1, 5 and 15 min at 65 °C (Figure 12 A). The RH and RF variants were the most resistant to proteolysis, while the HL and RL variants were significantly degraded after 5 min. The relative stabilities of the variants can be ordered as follows: RL < HL < HH < R < RF with $t_{1/2}$ at 65 °C of 1.3, 1.8, 2.2, 4.3 and 11 min, respectively.

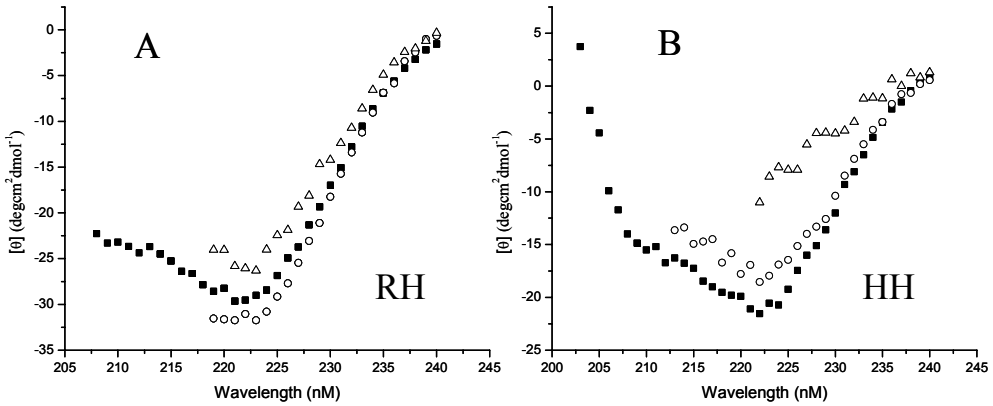

Figure 11: Comparison of secondary structure content at varying denaturant concentrations. Wavelength scans of the RH (panel A) and HH (panel B) enzymes at 0 (■), 0.75 (o) and 1.75 (Δ) M GdmCl as followed by circular dichroism. The RH enzyme displays an initial increase in secondary structure, whereas the HH displays a continual decrease at all denaturant concentrations.

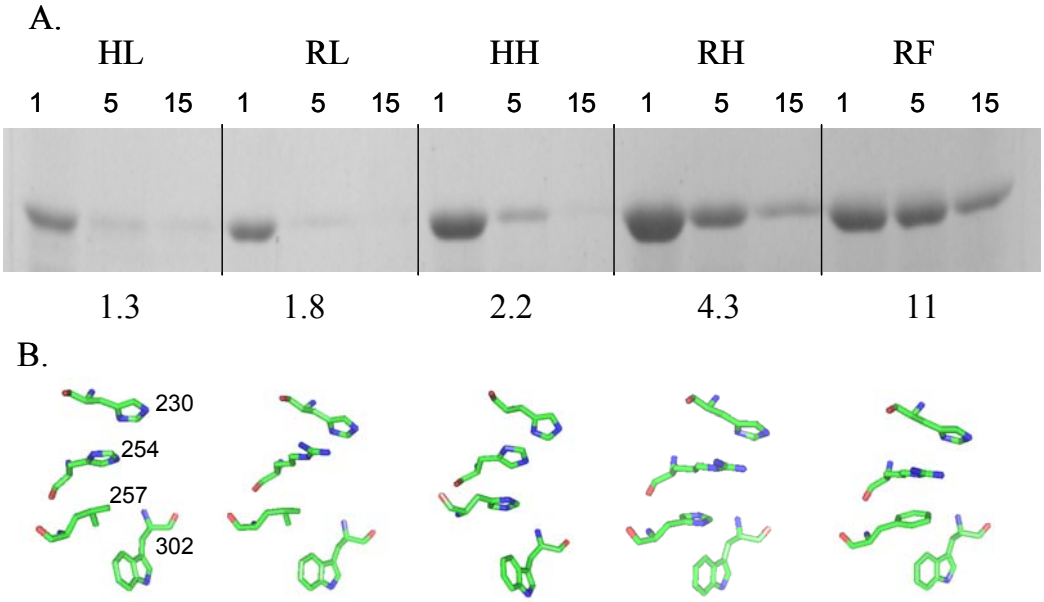

Figure 12: Thermolysin digest and structural comparison of the OPH variants.

A. Protease resistance to thermolysin at 65°C of the HL, RL, HH, RH and RF variants. The digestions were stopped at 1, 5 and 15 minute intervals by boiling the sample for 2 minutes in SDS loading buffer. Half lives in minutes are shown below each variant.

B. Relative positions of the side chains are shown for each variant. The backbone has been omitted for clarity. Comparison of the variants shows those that are the least stable have a leucine packed against W302. Those variants with an aromatic are more resistant to proteolysis.

Probing the tertiary structure

Whereas the mutations examined here all had enzymatic activities within an order of magnitude for the same substrates, the enzymes could be considered to have similar tertiary folded structures. This conclusion is supported by the recently published crystallographic structures of the RH and OPDA enzymes from our laboratory and others (72,78). The substitutions at positions 254 and 257 are in close proximity to W302, thus making tryptophan excitation a valuable tool for examining local changes in the tertiary structure. Selectively exciting the tryptophan residues at 295 nm revealed significant differences in the maximal emissions among the enzymes in the native states (Figure 13) suggesting the local environments of the tryptophans are dissimilar. The enzymes with the strongest tryptophan emissions were the HH and HL. The introduction of an arginine at position 254 resulted in a decrease and blue shift in signal, as seen in the RL and RH enzymes. Further quenching was seen with the addition of a phenylalanine at position 257, the RF variant. The changes in tryptophan emission among the variants suggested that the nature and proximity of residues 254 and 257 affected the emission of neighboring fluorophores, resulting in different spectra for similarly folded enzymes. These results further suggested that W302 was primarily responsible for the signal detected in the $N_2 \leftrightarrow I_2$ transition.

Another way to monitor conformational changes in proteins is to expose them to ANS (8-anilino-1-naphthalenesulfonic acid), which binds to hydrophobic regions of proteins in solution. ANS emission was observed to be maximal at a point that coincided with the minimum in the fluorescence emission between 1 and 2 M GdmCl in

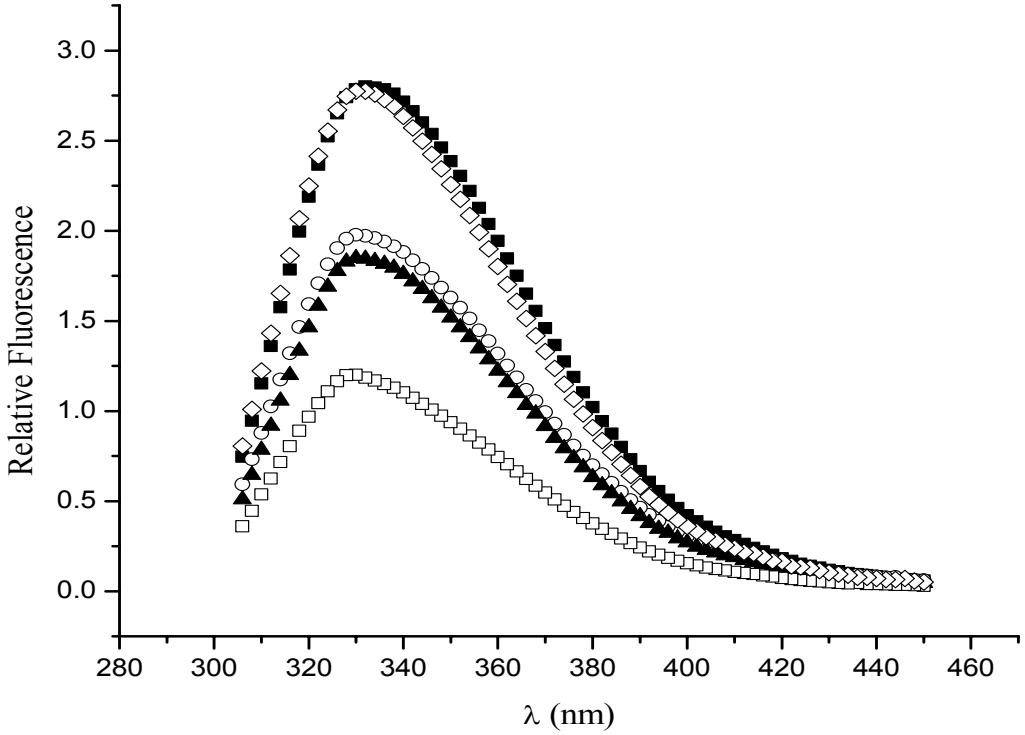

Figure 13: Selective excitation of tryptophan residues at 295 nm of the HH, HL, RH, RL and RF variants. HH (open diamonds), HL (filled squares), RL (filled triangles), RH (open circles), RF (open squares), at 100µg/ml protein. The HH and HL have the highest emission and an arginine present at position 254 results in quenching of fluorescence emission. The combination of an arginine at position 254 and a phenylalanine at position 257 result in the maximum emission decrease. Also present in the spectra is a blue shift coincident with a decrease in emission indicating burial of the fluorophore.

the RH and RF variants. This finding suggested that the RH and RF variants have a solvent accessible hydrophobic region at these denaturant concentrations that is absent from other variants (Figure 14).

Coumarin is a non-hydrolysable competitive inhibitor of OPH. It was used to determine if the ANS was binding in or near the active site. There was a significant decrease in ANS fluorescence in the presence of coumarin (Figure 15). This result suggested that the ANS was displaced by the inhibitor and that the formation of a hydrophobic pocket involves structural components near the active site. These data also support the blue shift seen in the tryptophan excitation, which would be expected if the rearrangement of structure reduced the amount of solvent accessible surface area of W302 (Figure 13).

Kinetic comparison with nerve agents

Comparison of the kinetics of the variant enzymes verified that RF exhibited the desired substrate profile of the other R254 enzymes, having a k_{cat} of 34 s^{-1} with the P-S substrate demeton-S (V agent surrogate). This increased activity with demeton-S was accompanied by a corresponding decrease in paraoxon activity with a k_{cat} of 448 s^{-1}. The k_{cat} of the RF variant with demeton-S was 10-fold greater than that of HH. This activity level was approximately equal to that of the RH enzyme, and was 60% as active as the RL variant (Table 7). Due to limited V agent availability and concentration ranges, only those enzymes with the desired demeton-S profiles were tested with these OP nerve agents. In addition, saturation of the enzymes with V agents was not possible because

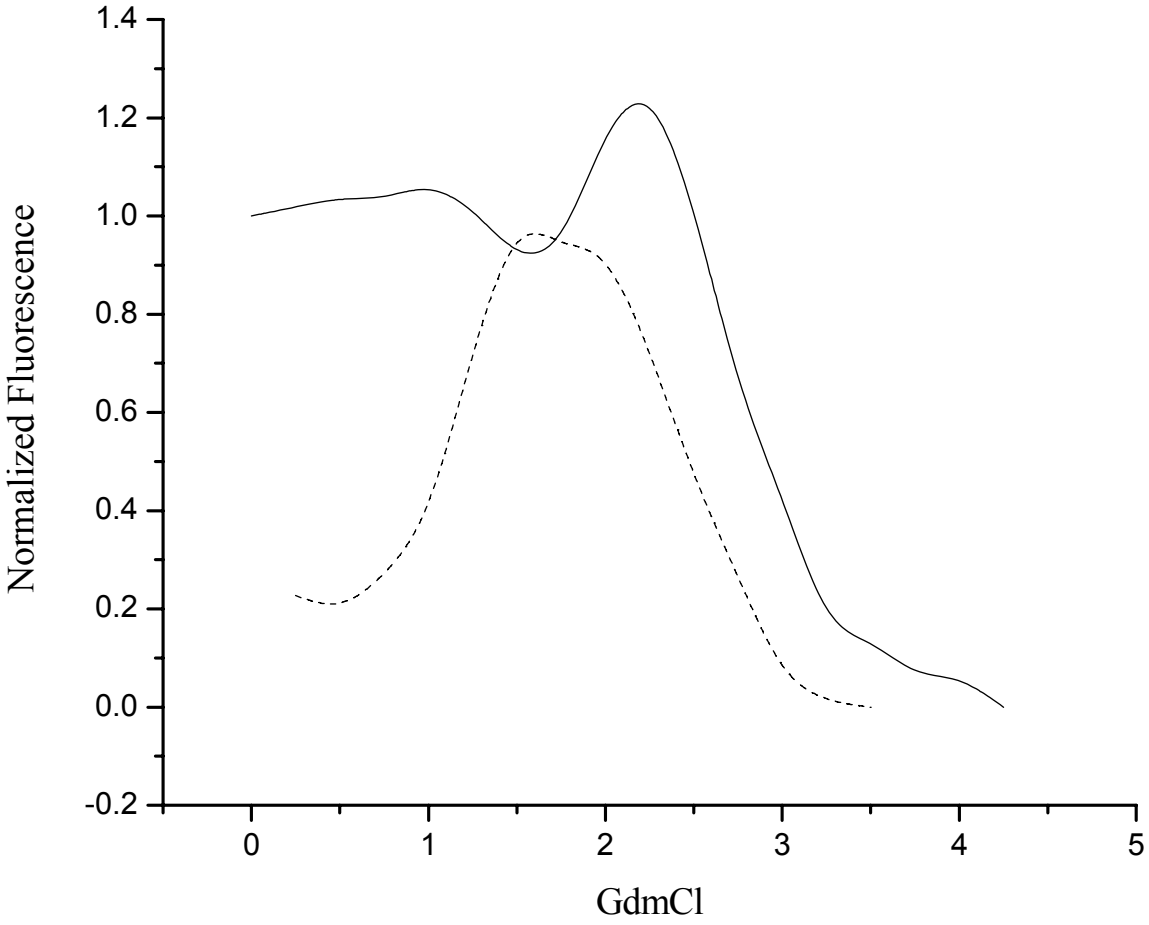

Figure 14: Comparison of RH fluorescence and ANS emission during GdmCl denaturation. Normalized fluorescence of the RH variant (solid line) and 50 μM ANS (dashed line) at the corresponding GdmCl concentrations. There is a maximum in ANS emission that corresponds to a local minimum in enzyme fluorescence indicating formation a hydrophobic pocket on the enzyme.

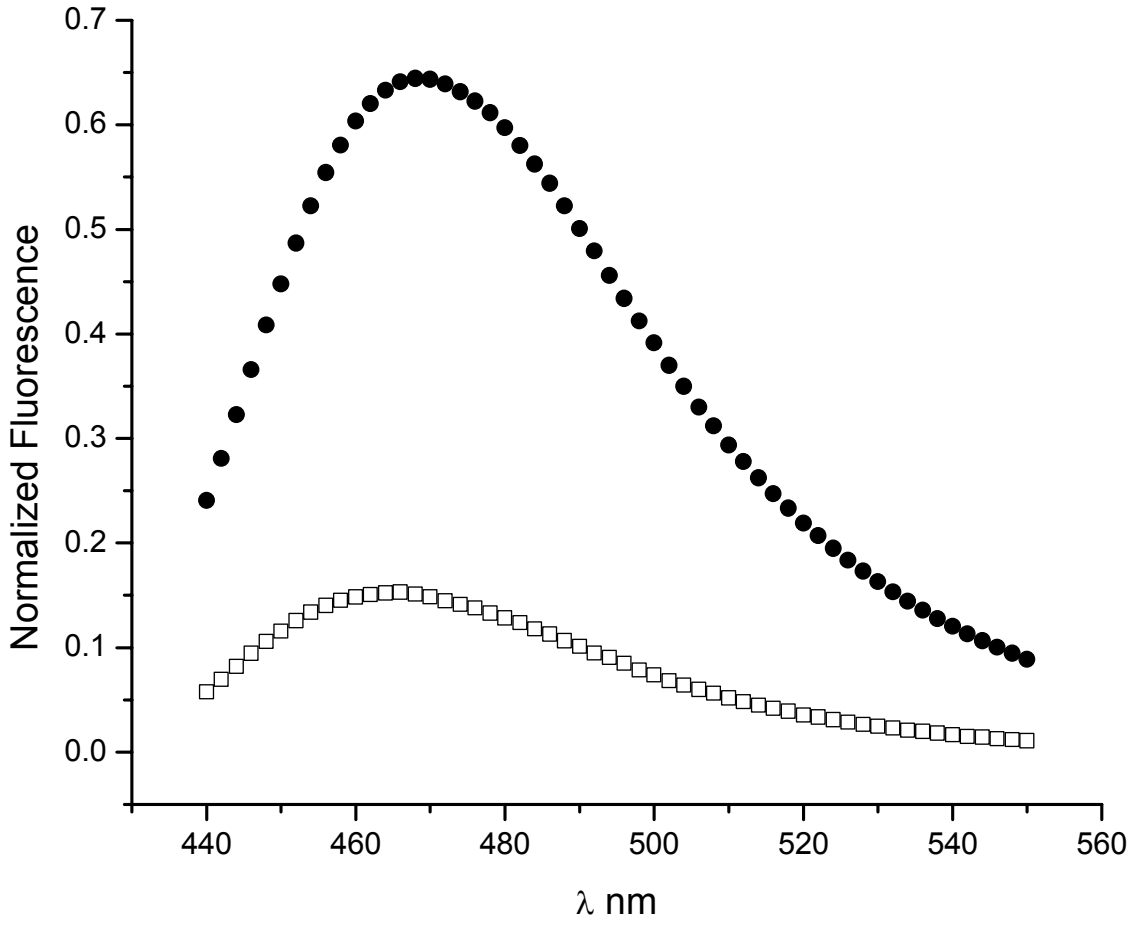

Figure 15: ANS displacement by coumarin. Fluorescence emission spectra of ANS/OPH at 1.5 M GdmCl in the presence of coumarin (□) and in the absence(●). Coumarin is a competitive inhibitor of the enzyme and binds in the active. The decrease in ANS emission could result from its displacement from in or near the active site.

of concentration limitations with surety materials. Under these conditions, the RL variant was the most effective enzyme for hydrolysis of VX and VR, with specific activities of 144 and 465 s^{-1} respectively. This is a 10X and 39X increase over the rates of the HH enzyme, 14 and 12 s^{-1}, for VX and VR, respectively. The RF variant had a kinetic profile that was intermediate to the HH and RL enzymes for these P-S bond V agents, with k_{cat} values of 68 and 36 s^{-1}, respectively. At concentrations of 2 mM agent and below, the enzymes are not saturated, so it is not clear if the increase in activity was a result of a change in the catalytic constant or substrate affinity. Lineweaver-Burke analysis of the data yielded large errors in K_M and was considered unreliable. Demeton-S profiles, under saturating conditions for the RF and RL enzymes, had large increases in k_{cat} relative to wildtype OPH (Table 7).

The comparative BuchE protection by OPH is shown in Figure 16. The RF variant was least effective against soman and cyclosarin. The limited substrate quantities and concentrations made it difficult to do detailed kinetic analysis and the G agent data presented here should be considered qualitative.

Structural analysis and variant design for surface attachment

The solvent accessible surface area (SASA) of the lysine residues in OPH are compared to the percent burial of the ζ-N, since examination of total SASA may not accurately predict the likelihood of biotinylation (Table 8). If the axis of the lysine side chain is perpendicular to the surface of the enzyme, the ζ-N will be completely exposed and have a higher probability of being biotinylated. However, when the axis is parallel

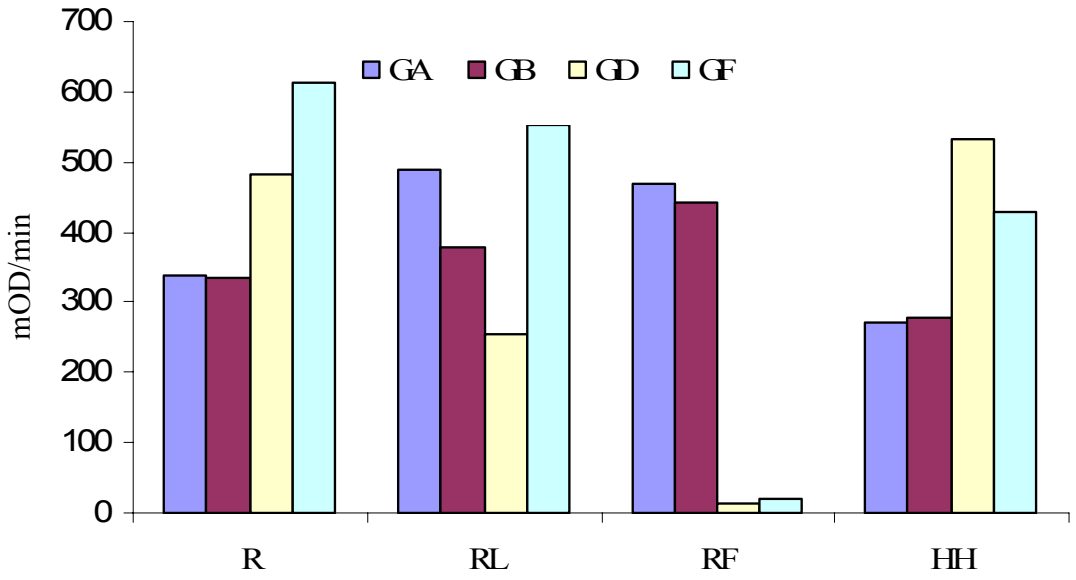

Figure 16: Comparative activity of Butyrylcholinesterase after the agents have been incubated with OPH variants for 6 hours. All the OPH enzyme show some degradation of the G agents. All variants showed improved hydrolysis of GA and GB when compared to the HH. The RF variant has a marked decrease in GD and GF hydrolysis in relation to the other enzymes.

Table 8: Solvent accessible surface area of OPH lysine residues.
Values in square angstroms and % burial of the zeta nitrogen

Residue #	Hydrophobic	Hydrophilic	Total SASA*	ζ – N burial**
169	11.8	10.4	22.2	99.1
82	48.2	13.5	61.7	53.9
285	37.2	29.6	66.8	26.1
185	33.2	36.3	69.5	21.9
339	42.7	58.4	101.2	26.7
77	94.4	54.9	149.3	14.3
294	102.3	63.0	165.3	-6.4
175	142.4	67.2	209.6	-8.2

* Determined by POPS (79).

** Determined by *pfis* (80).

to the enzyme surface, the ζ-N can be partially buried and inaccessible. Two of eight lysine residues in OPH can be considered inaccessible. K169 is carboxylated and is over 99% buried in the active site where it serves as a bridging ligand for the binuclear metal center. K82 is a surface residue; however, the ζ-N is more than 50% buried with the axis of the side chain being parallel to the surface of the enzyme. The remaining six lysines are over twice as accessible, and thus more probable attachment sites. Parameter optimized surfaces analysis (POPS) (79) of OPH shows that that K175 has the most SASA, at 209.6 square angstroms (Table 8). The percent burial of the ζ-N of K175 was calculated by *pfis* to be -8.2%, compared to the model tripeptide, GKG, indicating a completely exposed side chain (80). Since K175 is on the active site face of the enzyme, removing this attachment site will prevent the enzyme from being immobilized with the active site facing the sensor surface (Figure 17). The K175A variant is kinetically similar to wild type in solution assays having a k_{cat} of 3100 s^{-1} and K_M of 0.079 mM with paraoxon, giving a catalytic efficiency of 6.2 E^7 compared to 1 E^8 for the wild type. It is more susceptible to substrate inhibition, with a K_I of 3.9 mM versus 17 mM for the wild type. The K175A enzyme has a k_{cat} of 2 s^{-1} and K_M of 3.1 mM for demeton-S, giving a catalytic efficiency of 558 compared to 870 for the wild type, and no observable substrate inhibition (Table 9 and Figure 18).

Surface construction and immobilized activity

The real time sensorgram of the surface construction illustrates the stages of surface construction and binding of the wild type and K175A enzymes (Figure 19).

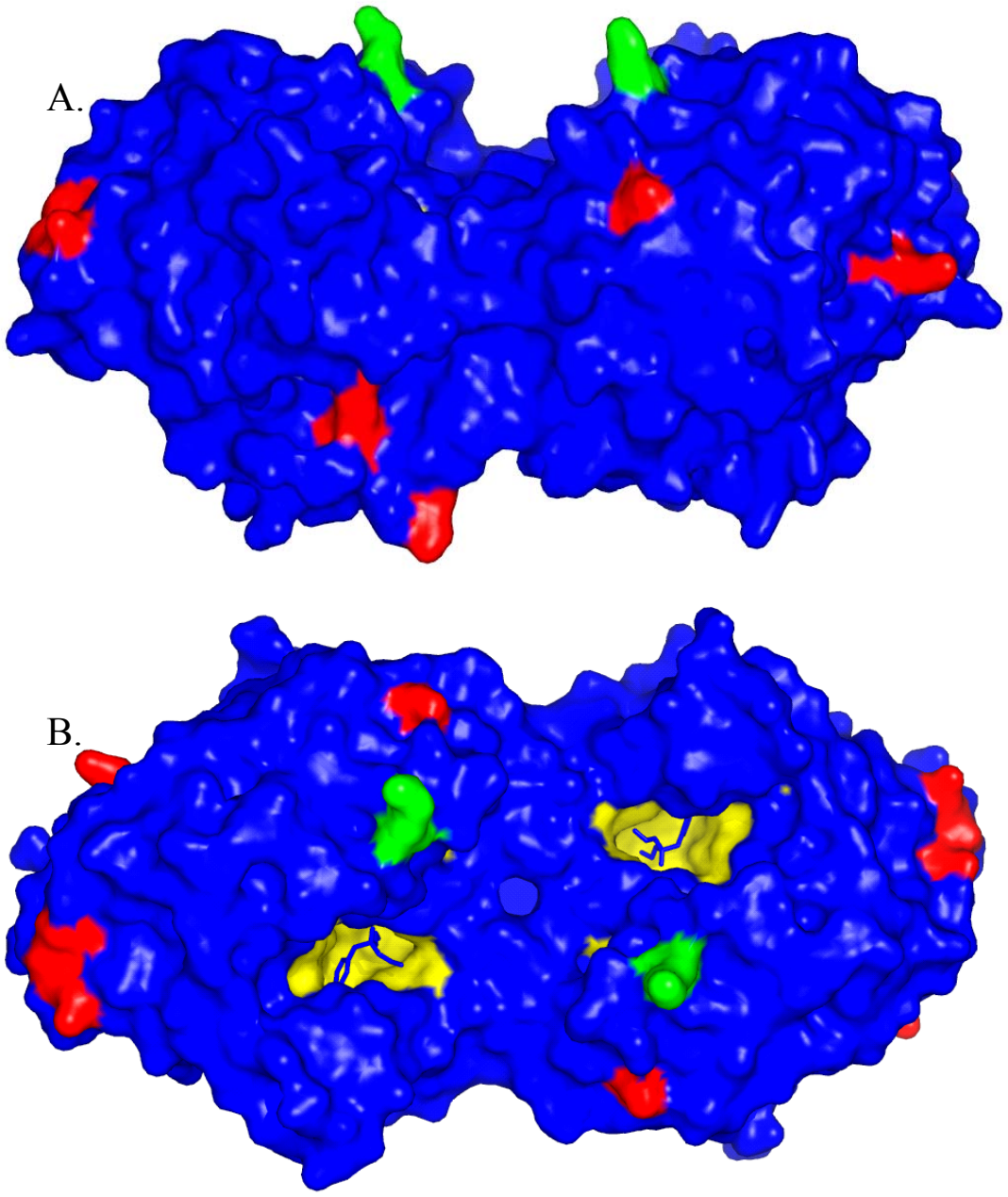

Figure 17: Solvent exposed lysine side chains of OPH. A. K175 is shown in green, others in red. B. The active site is shown in yellow to illustrate the proximity to K175.

Table 9: K175A kinetic parameters with paraoxon and demeton-S.

	Wild Type			K175A		
Substrate	k_{cat} s^{-1}	K_M mM	K_I mM	k_{cat} s^{-1}	K_M mM	K_I mM
Paraoxon	6900	0.08 ± 0.01	17 ± 2.1	3100	0.079 ± .016	3.9 ± 0.88
demeton-S	3.5	6.15 ± 1.75	NA	2	3.14 ± 0.6	NA

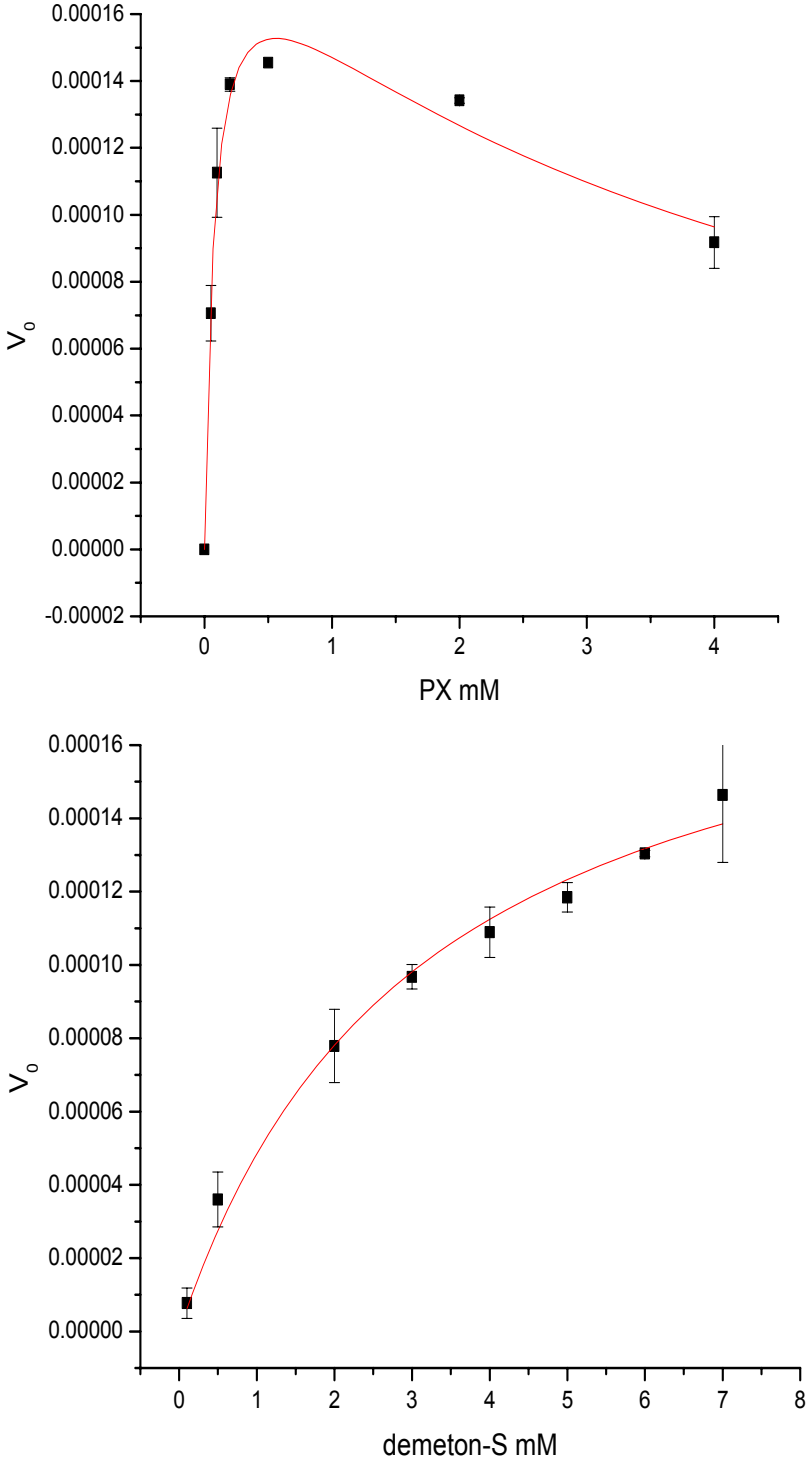

Figure 18: Substrate saturation curves for K175A with paraoxon and demeton-S. There is pronounced substrate inhibition with paraoxon at concentrations above 1 mM substrate.

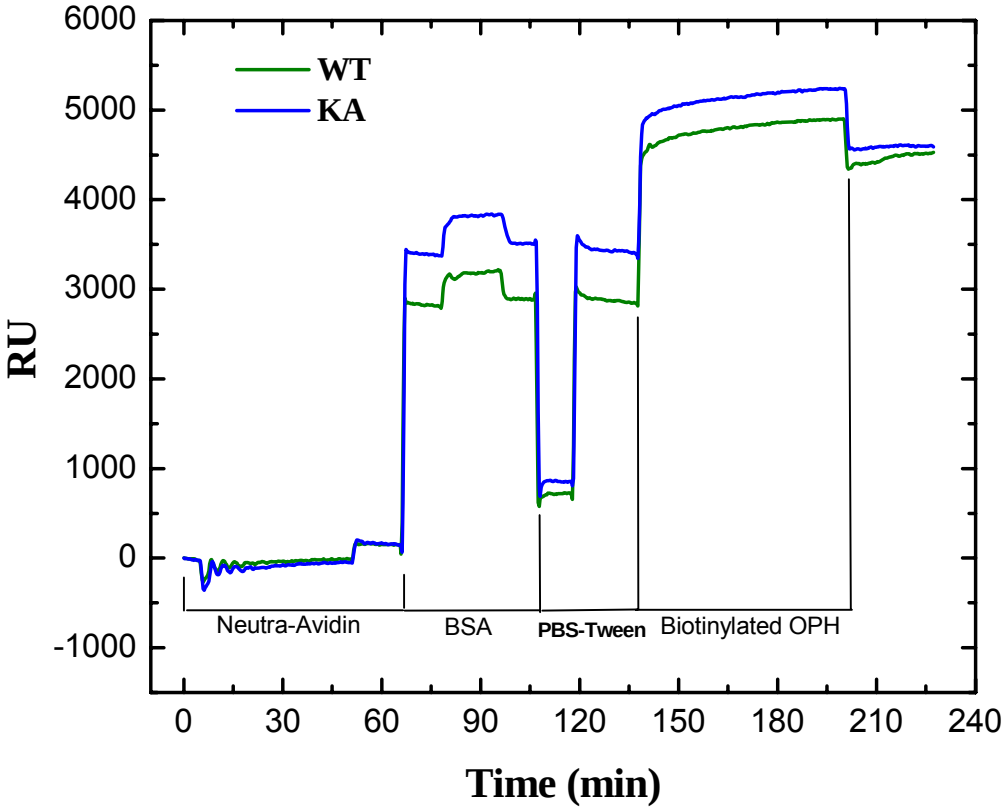

Figure 19: Real time sensogram of the SPR surface construction. The difference in response units (RU) shown on the Y axis is used to calculate the number of molecules deposited in each step allowing binding efficiencies of the proteins to be determined..

From the sensorgram, the surface coverage of the enzymes was calculated. The surface coverage at saturation in the K175A channel was found to be 3.17 E+09 molecules/mm^2 and 5.95 E+09 molecules/mm^2 for the WT channel. This indicates only 53.4% of the K175A molecules were immobilized compared to the wild type enzyme. The specific activity per mm^2 of immobilized K175A was 1.34 E-13 $\mu mol \cdot s^{-1}$ and the WT is 9.94 E-14 $\mu mol \cdot s^{-1}$ at a paraoxon concentration of 0.05 mM. There is a 2.5-3 fold enhancement of the surface efficiency.

Antibody coverage in the K175A channel was 8.39 E+8 molecules/mm^2 and 5.67 E+8 molecules/mm^2 for the WT channel. This results in a 1:3 ratio for antibody:K175A and a 1:10 ratio for the wild type.

DISCUSSION

Catalysis and stability

OPH is capable of hydrolyzing a variety of OP compounds containing P-O, P-F, P-CN and P-S bonds, with vastly different catalytic efficiencies. The activity of the native HH enzyme varied from the diffusion controlled limit with the P-O substrate paraoxon, with a k_{cat} of 6900 s^{-1}, to a catalytic rate as 4 s^{-1} with the P-S substrate demeton-S, resulting in a 1725 fold range in activity. The kinetics of the HL variant were similar to wild type OPH with demeton-S, while the RH single amino acid substitution increased activity with demeton-S four times over that of the native HH. The combination of the H254R and H257L substitutions in the RL variant resulted in demeton-S activity that was over 14 times that of the native HH (34) (Table 7). A comparison of the 257 and 254 variant activities indicated that an arginine substitution at position 254 was important for the increase in activity with phosphonothioate (P-S) substrates. The positively charged arginine at position 254 in the RH enzyme appeared to create a cation-π interaction between the parallel ring planes of H230 and the aromatic side chain at position 257. The planes of the aromatic rings are 7.7 angstroms from each other, placing the arginine, at most, 3.5 angstroms from either of the rings (72). The aliphatic leucine at position 257 in the HL and RL variants appears to disrupt an edge-to-face stacking interaction with W302 (Figure 12 B). The loss of this interaction had a significant effect on stability. Although the RL variant was very effective at hydrolyzing

P-S bonds, the increase in activity coincided with a loss of thermodynamic stability (Table 6).

Enzyme stability was proposed to correlate with the nature of the transition metal coordinated in the active site (Figure 20). The maximum catalytic activity was observed with the less stable Co^{2+} OPH. The trend in stability and metal content was similar to that seen in ACFII (42), where the charge to mass ratio was linear with stability. A smaller effective radius and higher charge to mass ratio, appeared to confer greater stability. H230 is a metal ligand which is intimately involved in structure function because of its association with residues 254 and 257. Flexibility in enzymes is important for catalytic function. Among the cobalt forms of OPH, RF was the most stable enzyme. If maximum activity was directly related to stability alone, this variant would have been expected to have the lowest activity, when in fact, it was intermediate to the less stable RL and HH wild type.

This study has indicated that cation-π and edge-to-face aromatic interactions involving residues 254 and 257 are important for stability and activity in OPH, particularly with P-S bond substrates. Cation-π interactions are common in proteins (81) and have been shown to be important structurally as well as for substrate binding and catalysis in various enzymes (82-85). Unlike stronger point charges such as salt bridges, the precise magnitudes of individual aromatic and cation-π interactions are difficult to calculate due to their complex nature and soluble structure characteristics. Aromatic residues, on the other hand, have the electrostatic potential distributed across an aromatic ring or ring system's π electron cloud. In cation-π interactions, charges from

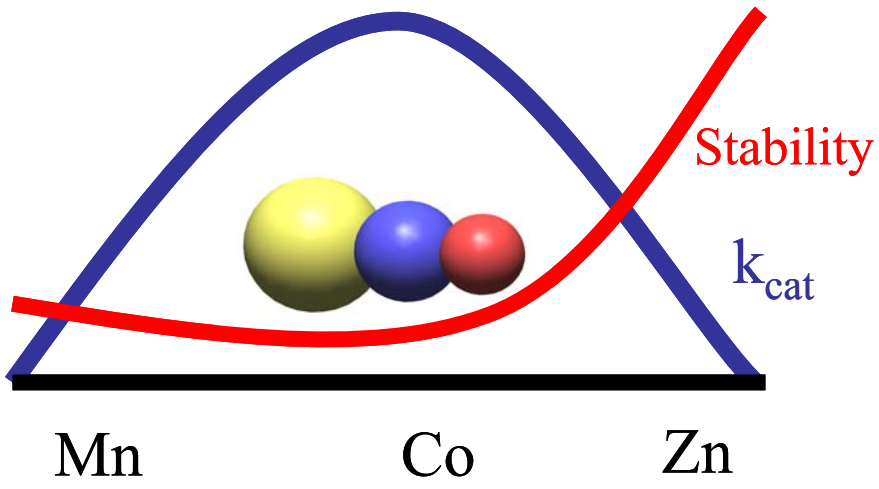

Figure 20: The relationship between stability and activity. In the HH enzyme, the most active form is not the most stable. Stability correlates with the charge to mass ratio of the transition metal coordinated in the enzyme.

neighboring residues affect the distribution of the electrostatic potential over the ring system and greatly affect the magnitude of the interaction. The contribution of various cation-π interactions to stability have been calculated to be 2-4 kcal/mol in proteins, with some estimates as high as 10 kcal/mol in the gas phase (85). The dominant forces and the magnitude of aromatic edge-to-face stacking interactions are under debate, but there is common agreement that these interactions contribute significantly to the stability of many proteins. An examination of the effects that side chain substituants have on the stability of the edge-to-face interaction has suggested that the dominant force is the electrostatic effect, which can provide up to 1.2 kcal/mol of stability (86). Other studies have suggested that London dispersion forces are the major component of the interaction, resulting in an induced dipole to provide the molecular attraction (87).

In order to balance conformational stability and catalytic activity, it appeared that creating an enzyme which preserved the P-S substrate activity of the 254R variants and the stability of the HH could be achieved by leaving the arginine at position 254 and replacing the leucine at position 257 with a phenylalanine. This substitution was predicted to reestablish the aromatic edge-to-face stacking with W302 found in the HH and RH enzymes. Indeed, the more hydrophobic phenylalanine is hypothesized to potentially provide a stronger interaction with W302 than the native histidine.

Assays with P-S substrates demonstrated that the RF variant possessed the desired activity profile with enhanced stability. Its activity with demeton-S, VX and VR was intermediate to the HH and RL enzymes and very similar to RH (Table 7). The activity of the RL variant might be attributed to increased flexibility of this region that

resulted from the loss of the stacking interaction between residues 257 and 302. This was synergistic with the introduction of the positively charged arginine at position 254. It has been suggested that the increase in activity resulted from an enlargement of the active site, allowing it to accommodate the bulkier P-S substrates (45). The active site is comprised of three distinct regions described as large, small and leaving group pockets (Figure 21) (44,59). Residue 257 is located at the boundary between the large pocket and the leaving group pocket. If the increase in activity was simply due to an enlargement of the large pocket, a more significant increase in demeton-S activity would have been expected in the HL variant.

Those variants which retained more structure at high temperature appeared to prevent localized unfolding, and possessed more restricted access to proteolysis sites, reducing degradation. The phenylalanine of the RF variant provided more stability than the histidines of the HH and RH enzymes (Figure 12A). In thermolysin digests at 65 °C, the RH and RF variants had half lives 2-5 times longer than that of the WT OPH. The stabilities from the thermolysin digests of RL, HL and wild type OPH correlated with those seen in the chemical denaturation experiments and supported the interpretation that RH and RF are more stable constructs. This suggested that the nature of the residue at position 257 played an important role in determining the stability of the enzyme. Variants with an aliphatic side chain at position 257 (RL and HL) were consistently the least stable, while those with an aromatic moiety were the most stable; the phenylalanine provided more stability to the enzyme than the less hydrophobic histidine (Figure 12B). The arginine at position 254 appeared to introduce a cation-π interaction between the

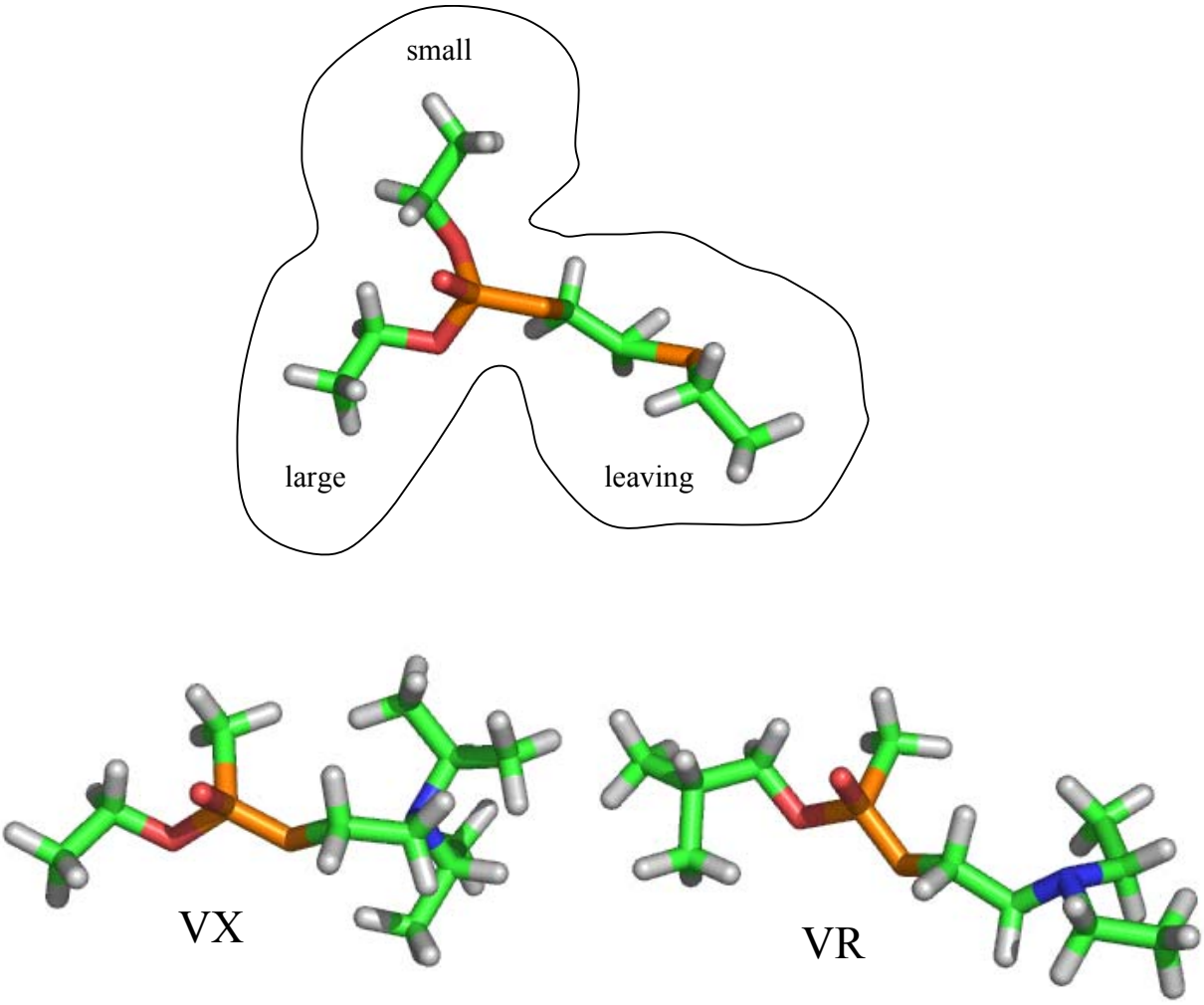

Figure 21: The binding pockets of the active site of OPH. The pockets are describes as the small, large, and the leaving group pocket. Demeton-S is shown bound in the active site outline and VX and VR are shown for reference.

histidine residues at positions 230 and 257 (PDB 1QW7) (72). This electrostatic interaction would be expected to provide an increase in stability over the purely hydrophobic aromatic stacking interactions found in the HH enzyme.

Unfolding model

It is possible to construct a model for the initial unfolding of OPH around the active site from the equilibrium denaturation and ANS data. A local minimum in the fluorescence signal prior to the $I_2 \leftrightarrow 2U$ transition was coincident with a maximum in the CD signal and ANS intensity, suggesting a rearrangement or compacting of the protein without a significant loss of structure at this point in the unfolding pathway. The displacement of ANS by coumarin suggested that near-active site regions are involved in the structural rearrangement, possibly helices 15 and 18 (Figure 22). Similar changes have been observed for other enzymes such as ribonuclease A and dihydrofolate reductase (DHFR), in which the loss of activity upon exposure to denaturants preceded any detectable global change in the protein (88). The local minimum in intrinsic tryptophan fluorescence at GdmCl concentrations between 1-2 M was proposed to result from R254 assuming closer proximity to W302 and quenching the fluorescence emission as the enzyme assumed a more compact or ordered overall structure (Figure 22). CD spectra at these denaturant concentrations supported this hypothesis, as the RF and RH enzymes exhibit greater secondary structure content when compared to the HH.

The importance of position 257 to the structural integrity of the enzyme and its effect on catalytic activity highlighted the importance of balancing the relationship

A. B.

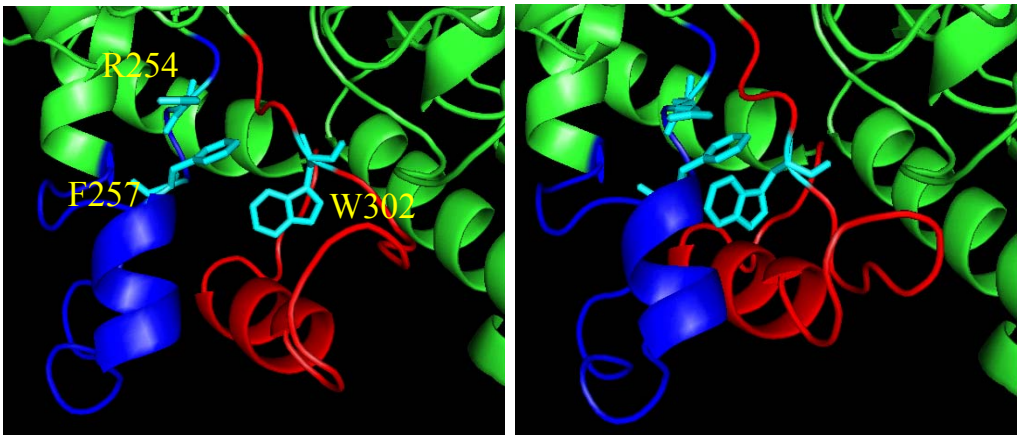

Figure 22: Modeled RF crystal structure based on the RH 1QW7 PDB structure (72). Panel A is the relative positions of R254, F257 and W302 in the native state. Panel B depicts the movement of helices 15 (blue) and 18 (red) to form a hydrophobic pocket and position residues 254 and 257 closer to W302.

between the flexibility and catalytic function. While the contribution of a single stacking interaction between residues 257 and 302 may appear to be small in magnitude, it occupied a location critical in determining the relative stability and substrate specificity of OPH. The RL and HL variants, with an aliphatic leucine in place of the native histidine at position 257, displayed a decrease of 5-6 kcal/mol in thermodynamic stability compared to the native HH enzyme. Aromatic networks can have large effects on the thermal stability of proteins, as well as their activity (89), and small variations in stability greatly affected the amount of protein in the native state near the $T_{M\ app}$ because of the cooperative nature of folding. Thus, even modest increases in stability would result in large shifts among the conformational populations of a protein ensemble. For example, at 27 °C both the HH and RL are over 99% in the folded form (Figure 23). At 66 °C the folded fractions were shifted to 28% for the RL and 80% for the HH. This observation emphasized the effect that small changes in stability can have on enzyme activity and conformation. In OPH, substituting one or two residues appeared to result in large changes in thermal stability.

Making small changes in the stability of a protein can result in large shifts in the folding equilibrium, resulting in a more functional enzyme. This can have significant implications in industrial applications, such as the disposal of CWA, where increasing the reaction temperature by only a few degrees can greatly affect the speed of hydrolysis by enzymes stable at higher temperatures. The combination of a cation-π interaction and more stable aromatic interaction in the RF variant resulted in an enzyme that was more stable than the HH, yet still had the more desirable catalytic characteristics with P-S

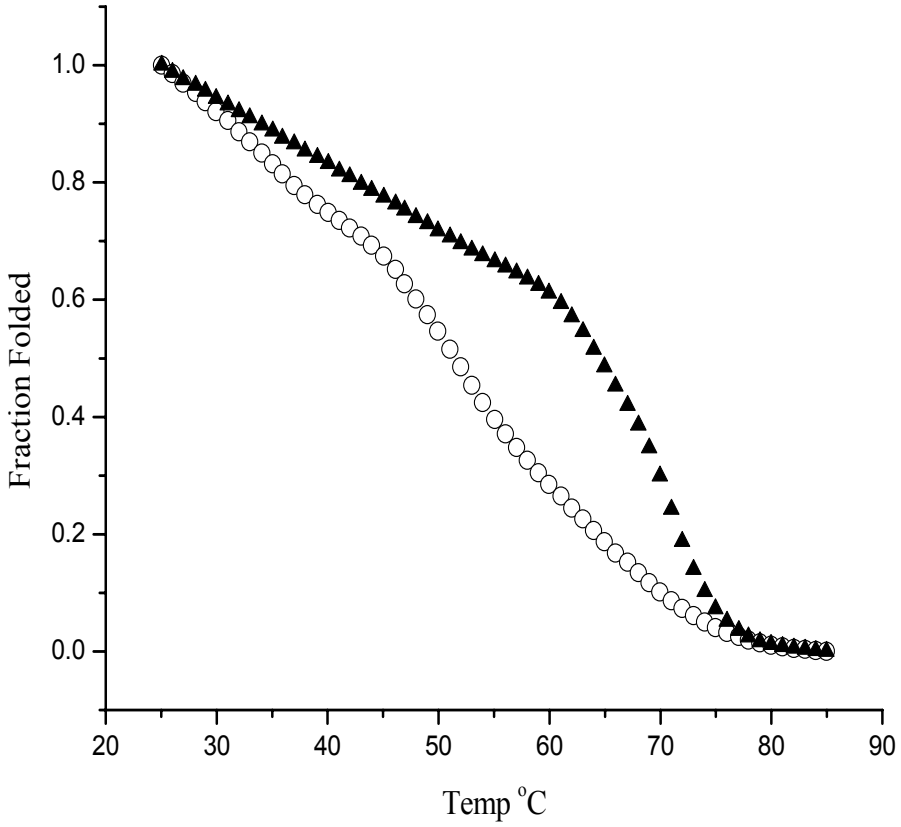

			Native Fraction	
Enzyme	k_{cat}·s^{-1}*	$T_{M\ app}$ ºC	27 ºC	66 ºC
RL	68	60	.991	.281
HH	5	71	.999	.791

* Activity with the VX analog demeton-S

Figure 23: Thermal denaturation of the HH and RL enzymes. HH (filled triangles) and RL (open circles) variant followed by intrinsic tryptophan fluorescence. The fraction in the native form for each variant is calculated at 27 and 66 °C.

substrates (including the nerve agents VX and VR). Using rational design of OPH and applying our understanding of side chain interactions, this study has shown that it was possible to increase the stability of an enzyme and retain desired catalytic properties.

Designing enzymes for developing reactive surfaces

Figure 24 depicts an attachment surface, where Neutravidin coats the gold surface and BSA and Tween block any unoccupied space. This construction restricted OPH immobilization to available avidin sites through a biotin linker. The most exposed surface lysine in OPH is K175 and its proximity to the active site could conceivably impede the movement of substrates and products in and out of the active site if the enzyme were immobilized "upside-down" through this side chain. On the basis that flexibility is important for catalytic activity, the physical restraint of secondary structure in this region could adversely affect catalysis.

If the replacement of K175 had no effect on the orientation of the immobilized enzymes, one would expect similar binding of antibodies to both the wild type and K175A enzyme surface, based on a random presentation of the epitopes. Polyclonal antibodies bind one in three immobilized K175A molecules, and they only bind one out of every ten WT enzymes. This finding suggested that the epitope was oriented differently when K175 was immobilized on the surface, in a more favorable orientation (e.g. "face-up"). The activity of an OPH-K175A biosensor is 25% higher that that of the WT. When the number of molecules per mm^2 is taken into account, the specific activity of the K175A surface is increased 2.5 fold. The increased efficiency could be the result

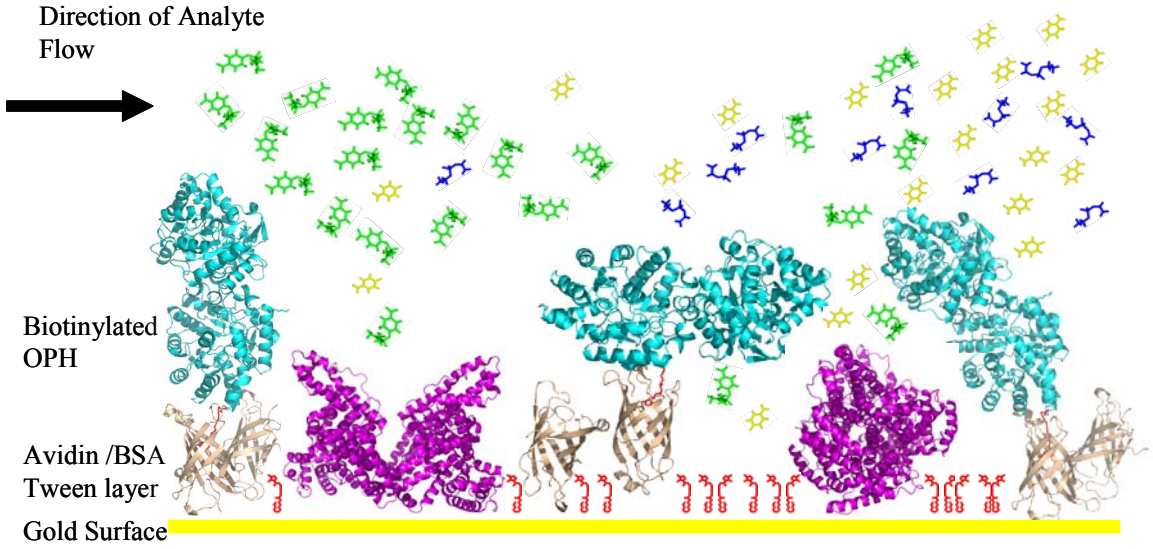

Figure 24: Layers of the surface plasmon resonance sensor.

of a more consistent orientation or more flexibility in the secondary structure near the active site (Figure 25).

Protein design considerations

The rational design of OPH for improved catalytic efficiency or substrate specificity has been successful for a variety of OP neurotoxins. Our knowledge of this enzyme's structure and mechanism made the selection of individual residues to achieve this possible. The utility of the enzyme in emerging technologies for CWA applications, such as immobilization on sensor surfaces, makes the study of these interactions important. Figure 26 illustrates the interactions of structural components as they relate to various enzyme characteristics.

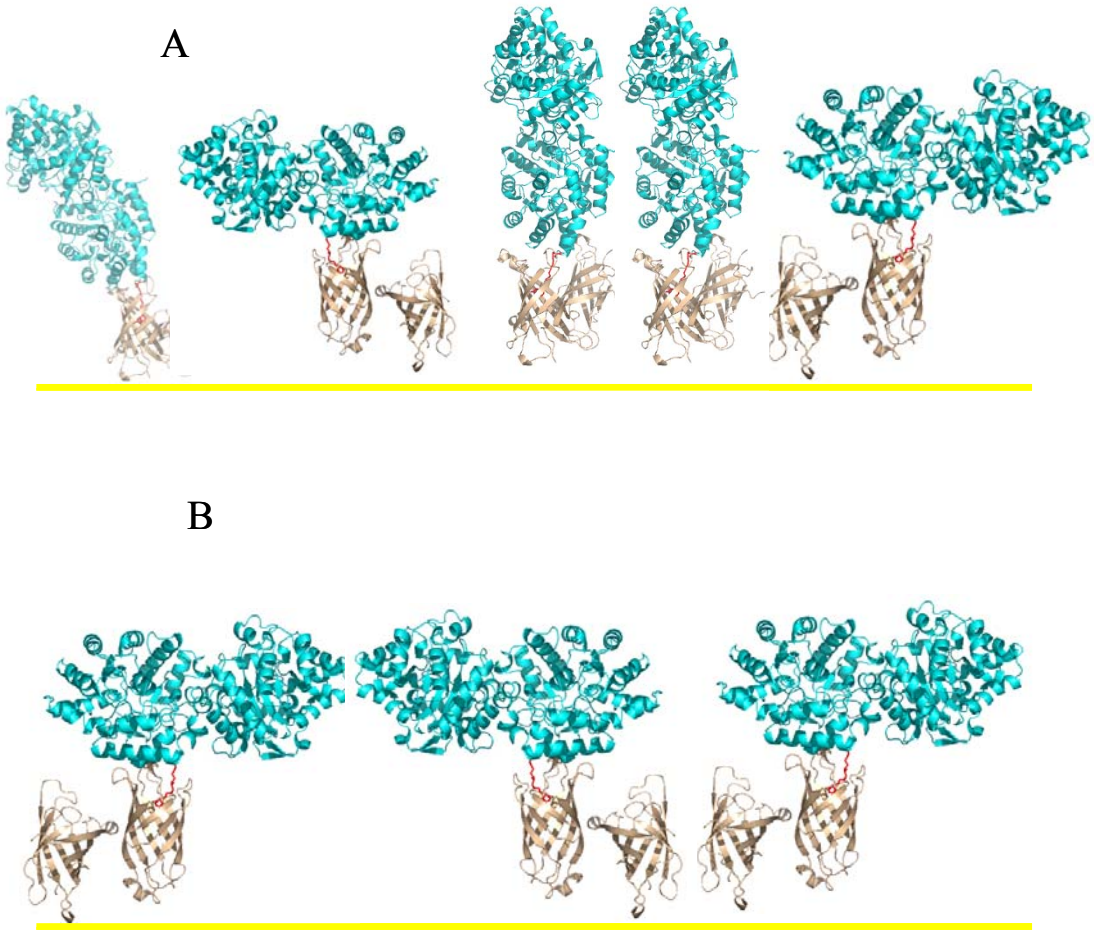

Figure 25: Model of an optimized surface. Panel A illustrates OPH (cyan) in an ensemble of orientations when immobilized to avidin (beige). Panel B depicts an ordered surface.

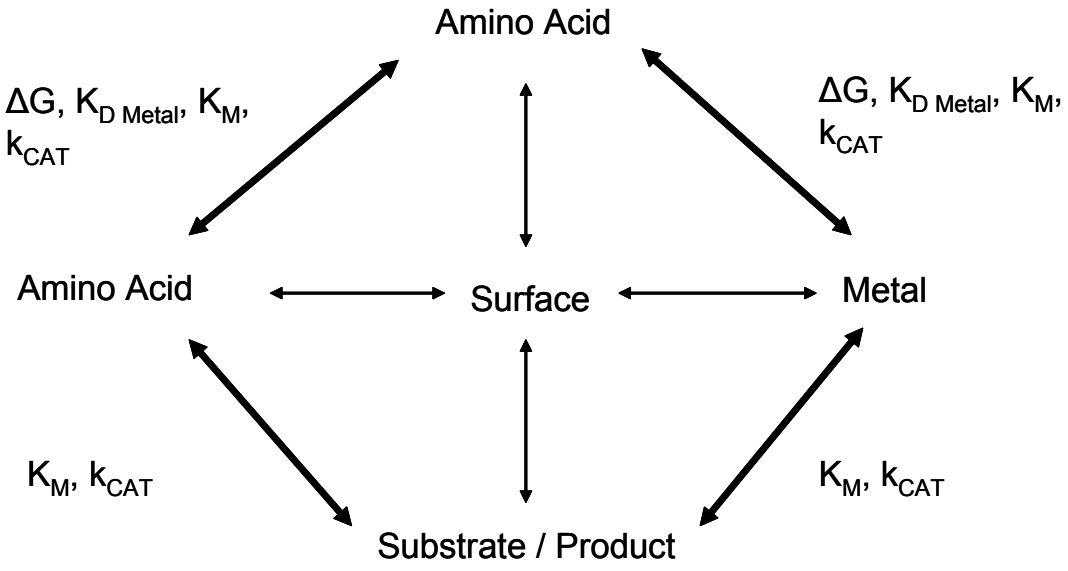

Figure 26: Protein design considerations showing the interaction of various components involved in enzyme stability and activity. In this example the application would be for surface attachment, so it is necessary to consider how substitutions of a side chain would affect other enzyme/protein characteristics.

CONCLUSIONS

Rational site-directed mutagenesis and equilibrium unfolding experiments have been used to explore the integrated roles of residues 254 and 257 in the global stability and catalytic specificities of organophosphorus hydrolase (OPH, EC 3.1.8.1). Substitution of residues H254 and H257, which are located near the active site, had a marked effect on both the global stability and substrate specificity of the enzyme. For example, the ΔG_T for the second generation H254R H257L (RL) enzyme variant was 19.6 kcal/mol, 5.7 kcal/mol less than that of the wild type enzyme. At the same time, the enzyme was catalytically more effective against VX and VR (Russian VX), as compared to the wild type enzyme. Limited proteolysis profiles verified the importance of residues 254 and 257 for stability, evidenced by enhanced resistance to unfolding associated with thermal denaturation. Rational design has made possible the construction of OPH variants which are more stable than the wild type enzyme, and still retain desirable catalytic properties. Aromatic stacking and cation-π interactions near the active site appear to affect activity and significantly contribute to the chemical and thermal stability of OPH.

Covalent attachment methods to immobilize enzymes take advantage of amino acid side chains, typically lysines and cysteines. The random distribution of solvent exposed side chains on an enzyme results in an ensemble of orientations when the protein is immobilized on a surface or in a matrix through side chain linkages. Depending on the attachment mechanism, this random orientation could restrict product and substrate access to and from the active site. This study presents an orientation

specific attachment of the enzyme to a surface plasmon resonance (SPR) cell surface, in order to optimize active site accessibility, and thus enhance sensitivity of instruments. The substitution of the surface lysine K175 removed biotinylation sites on the active site face of the enzyme dimer, preventing immobilization with the active sites oriented toward the sensor surface. Kinetic comparison of the enzymes in solution demonstrates that the K175A variant retained 80% of the WT activity with the pesticide substrates paraoxon and demeton-S in solution. However, after immobilization, activity assays showed that K175A surfaces were 20% more active, with 53% fewer molecules bound per mm^2, when compared to a wild type enzyme surface. This increase resulted in a surface activity that is 2.5 to 3-fold more efficient. Antibody recognition of the enzyme immobilized on a SPREETA sensor surface demonstrated a three fold preference for the K175A enzyme, indicating a difference between the enzymes in accessibility of the antibody binding epitope. These data indicate that orientation of the enzyme is important for enzyme functionality on the sensor surface and should provide a basis for optimization when using enzymes as the bio-recognition element.

REFERENCES

1. Holmstedt, B. (1991) Historical Perspective and Future of Ethnopharmacology, *J. Ethnopharmacol. 32*, 7-24.

2. LangW and von Kruger G. (1932) Uber Ester Der Monofluorophosphorsaure, *Ber Dtsch Chem Ges 65*, 1598-1601.

3. Schrader G (1950) Organische Phosphor-Uberbindun-Gen Als Neuratige Insekticide, *Angew Chem* 471-473.

4. Palmer T and Taylor P (1996) The Pharmacological Basis of Therapeutics, *Toxicology Letters 55,* 161-176.

5. Gutmann, L. and Besser, R. (1990) Organophosphate Intoxication: Pharmacologic, Neurophysiologic, Clinical, and Therapeutic Considerations, *Semin. Neurol. 10*, 46-51.

6. Moretto, A. and Lotti, M. (2002) The Relationship Between Isofenphos Cholinergic Toxicity and the Development of Polyneuropathy in Hens and Humans, *Arch. Toxicol. 76*, 367-375.

7. Senanayake, N. and Johnson, M. K. (1982) Acute Polyneuropathy After Poisoning by a New Organophosphate Insecticide, *N. Engl. J. Med. 306*, 155-157.

8. National Security and International Affairs Division (2006) Department of Defense, Need for Chemical Suits and Masks; B-247350, United States General Accounting Office, Washington D.C.

9. Beards, S. C., Kraus, P., and Lipman, J. (1994) Paralytic Ileus As a Complication of Atropine Therapy Following Severe Organophosphate Poisoning, *Anaesthesia 49*, 791-793.

10. Fisher, C. M. (1991) Visual Hallucinations on Eye Closure Associated With Atropine Toxicity. A Neurological Analysis and Comparison With Other Visual Hallucinations, *Can. J. Neurol. Sci. 18*, 18-27.

11. Jaeger, K. E. and Eggert, T. (2002) Lipases for Biotechnology, *Curr. Opin. Biotechnol. 13*, 390-397.

12. Parales, R. E. and Haddock, J. D. (2004) Biocatalytic Degradation of Pollutants, *Curr. Opin. Biotechnol. 15*, 374-379.

13. Cherry, J. R. and Fidantsef, A. L. (2003) Directed Evolution of Industrial Enzymes: an Update, *Curr. Opin. Biotechnol. 14*, 438-443.

14. Piao, H., Marx, R. B., Schneider, S., Irvine, D. A., and Staton, J. (2005) Analysis of VX Nerve Agent Hydrolysis Products in Wastewater Effluents by Ion Chromatography With Amperometric and Conductivity Detection, *J. Chromatogr. A 1089*, 65-71.

15. Szafraniec, L. J., Szafraniec, L. L., Beaudry, W. T., and Ward, J. R. (1990) *On the Stoichiometry of Phosphonothiolate Ester Hydrolysis*, *CRDEC-TR-212*.

16. Kononova, S. V. and Nesmeyanova, M. A. (2002) Phosphonates and Their Degradation by Microorganisms, *Biochemistry (Mosc.) 67*, 184-195.

17. Wanner, B. L. and Metcalf, W. W. (1992) Molecular Genetic Studies of a 10.9-Kb Operon in Escherichia Coli for Phosphonate Uptake and Biodegradation, *FEMS Microbiol. Lett. 79*, 133-139.

18. Garden, J. M., Hause, S. K., Hoskin, F. C. G., and Roush, A. H. (1975) Comparison of Dfp-Hydrolyzing Enzyme Purified From Head Ganglion and Hepatopancreas of Squid (Loligo-Pealei) by Means of Isoelectric Focusing, *Comparative Biochemistry and Physiology C-Pharmacology Toxicology & Endocrinology 52*, 95-98.

19. Mazur, A. (1946) An Enzyme in the Animal Organism Capable of Hydrolyzing Diisopropyl Fluorophosphate, *Federation Proceedings 5*, 147.

20. Mulbry, W. W., Karns, J. S., Kearney, P. C., Nelson, J. O., McDaniel, C. S., and Wild, J. R. (1986) Identification of A Plasmid-Borne Parathion Hydrolase Gene From Flavobacterium Sp by Southern Hybridization With Opd From Pseudomonas-Diminuta, *Applied and Environmental Microbiology 51*, 926-930.

21. Zheng, J., Constantine, C. A., Zhao, L., Rastogi, V. K., Cheng, T. C., Defrank, J. J., and Leblanc, R. M. (2005) Molecular Interaction Between Organophosphorus Acid Anhydrolase and Diisopropylfluorophosphate, *Biomacromolecules 6*, 1555-1560.

22. Cheng, T. C., Rastogi, V. K., Defrank, J. J., and Sawiris, G. P. (1998) G-Type Nerve Agent Decontamination by Alteromonas Prolidase, *Ann. N. Y. Acad. Sci. 864*, 253-258.

23. Chettur, G., Defrank, J. J., Gallo, B. J., Hoskin, F. C., Mainer, S., Robbins, F. M., Steinmann, K. E., and Walker, J. E. (1988) Soman-Hydrolyzing and -Detoxifying Properties of an Enzyme From a Thermophilic Bacterium, *Fundam. Appl. Toxicol. 11*, 373-380.

24. Wang, F., Xiao, M., and Mu, S. (1993) Purification and Properties of a Diisopropyl-Fluorophosphatase From Squid Todarodes Pacificus Steenstrup, *J. Biochem. Toxicol. 8*, 161-166.

25. Scharff, E. I., Koepke, J., Fritzsch, G., Lucke, C., and Ruterjans, H. (2001) Crystal Structure of Diisopropylfluorophosphatase From Loligo Vulgaris, *Structure 9*, 493-502.

26. Harel, M., Aharoni, A., Gaidukov, L., Brumshtein, B., Khersonsky, O., Meged, R., Dvir, H., Ravelli, R. B., McCarthy, A., Toker, L., Silman, I., Sussman, J. L., and Tawfik, D. S. (2004) Structure and Evolution of the Serum Paraoxonase Family of Detoxifying and Anti-Atherosclerotic Enzymes, *Nat. Struct. Mol. Biol. 11*, 412-419.

27. Kuo, C. L. and La Du, B. N. (1998) Calcium Binding by Human and Rabbit Serum Paraoxonases. Structural Stability and Enzymatic Activity, *Drug Metab Dispos. 26*, 653-660.

28. Kuo, C. L. and La Du, B. N. (1995) Comparison of Purified Human and Rabbit Serum Paraoxonases, *Drug Metab Dispos. 23*, 935-944.

29. Davies, H. G., Richter, R. J., Keifer, M., Broomfield, C. A., Sowalla, J., and Furlong, C. E. (1996) The Effect of the Human Serum Paraoxonase Polymorphism Is Reversed With Diazoxon, Soman and Sarin, *Nat. Genet. 14*, 334-336.

30. Yeung, D. T., Lenz, D. E., and Cerasoli, D. M. (2005) Analysis of Active-Site Amino-Acid Residues of Human Serum Paraoxonase Using Competitive Substrates, *FEBS J. 272*, 2225-2230.

31. Harper, L. L., McDaniel, C. S., Miller, C. E., and Wild, J. R. (1988) Dissimilar Plasmids Isolated From Pseudomonas Diminuta MG and a Flavobacterium Sp. (ATCC 27551) Contain Identical Opd Genes, *Appl. Environ. Microbiol. 54*, 2586-2589.

32. McDaniel, C. S., Harper, L. L., and Wild, J. R. (1988) Cloning and Sequencing of a Plasmid-Borne Gene (Opd) Encoding a Phosphotriesterase, *J. Bacteriol. 170*, 2306-2311.

33. Aubert, S. D., Li, Y., and Raushel, F. M. (2004) Mechanism for the Hydrolysis of Organophosphates by the Bacterial Phosphotriesterase, *Biochemistry 43*, 5707-5715.

34. Di Sioudi, B. D., Miller, C. E., Lai, K., Grimsley, J. K., and Wild, J. R. (1999) Rational Design of Organophosphorus Hydrolase for Altered Substrate Specificities, *Chem. Biol. Interact. 119-120*, 211-223.

35. Dudev, T. and Lim, C. (2003) Principles Governing Mg, Ca, and Zn Binding and Selectivity in Proteins, *Chem Rev. 103*, 773-788.

36. Danel, F., Paetzel, M., Strynadka, N. C., and Page, M. G. (2001) Effect of Divalent Metal Cations on the Dimerization of OXA-10 and -14 Class D Beta-Lactamases From Pseudomonas Aeruginosa, *Biochemistry 40*, 9412-9420.

37. Dirnbach, E., Steel, D. G., and Gafni, A. (2001) Mg2+ Binding to Alkaline Phosphatase Correlates With Slow Changes in Protein Lability, *Biochemistry 40*, 11219-11226.

38. Dudev, T., Lin, Y. L., Dudev, M., and Lim, C. (2003) First-Second Shell Interactions in Metal Binding Sites in Proteins: a PDB Survey and DFT/CDM Calculations, *J. Am. Chem Soc. 125*, 3168-3180.

39. Lai, K. H., Dave, K. I., and Wild, J. R. (1994) Bimetallic Binding Motifs in Organophosphorus Hydrolase Are Important for Catalysis and Structural Organization, *Journal of Biological Chemistry 269*, 16579-16584.

40. Shim, H. and Raushel, F. M. (2000) Self-Assembly of the Binuclear Metal Center of Phosphotriesterase, *Biochemistry 39*, 7357-7364.

41. Grimsley, J. K., Scholtz, J. M., Pace, C. N., and Wild, J. R. (1997) Organophosphorus Hydrolase Is a Remarkably Stable Enzyme That Unfolds Through a Homodimeric Intermediate, *Biochemistry 36*, 14366-14374.

42. Xu, X. L. (2006) Effects of Rare Earth Ions on The Conformational Stability of Anticoagulation Factor II From Agkistrodon Actus Venom Probed by Fluorescent Spectroscopy., *Bioploymers*(in press).

43. Millard, C. B., Lockridge, O., and Broomfield, C. A. (1998) Organophosphorus Acid Anhydride Hydrolase Activity in Human Butyrylcholinesterase: Synergy Results in a Somanase, *Biochemistry 37*, 237-247.

44. Chen-Goodspeed, M., Sogorb, M. A., Wu, F. Y., and Raushel, F. M. (2001) Enhancement, Relaxation, and Reversal of the Stereoselectivity for Phosphotriesterase by Rational Evolution of Active Site Residues, *Biochemistry 40*, 1332-1339.

45. Lai, K. H., Grimsley, J. K., Kuhlmann, B. D., Scapozza, L., Harvey, S. P., DeFrank, J. J., Kolakowski, J. E., and Wild, J. R. (1996) Rational Enzyme

Design: Computer Modeling and Site-Directed Mutagenesis for the Modification of Catalytic Specificity in Organophosphorus Hydrolase, *Chimia 50*, 430-431.

46. Liu, X. S. and Dean, D. H. (2006) Redesigning Bacillus Thuringiensis Cry1Aa Toxin into a Mosquito Toxin, *Protein Eng Des Sel 19*, 107-111.

47. Kaneko, H., Minagawa, H., and Shimada, J. (2005) Rational Design of Thermostable Lactate Oxidase by Analyzing Quaternary Structure and Prevention of Deamidation, *Biotechnol. Lett. 27*, 1777-1784.

48. Arnold, F. H., Giver, L., Gershenson, A., Zhao, H., and Miyazaki, K. (1999) Directed Evolution of Mesophilic Enzymes into Their Thermophilic Counterparts, *Ann. N. Y. Acad. Sci. 870*, 400-403.

49. Miyazaki, K. and Arnold, F. H. (1999) Exploring Nonnatural Evolutionary Pathways by Saturation Mutagenesis: Rapid Improvement of Protein Function, *J. Mol. Evol. 49*, 716-720.

50. Miyazaki, K., Wintrode, P. L., Grayling, R. A., Rubingh, D. N., and Arnold, F. H. (2000) Directed Evolution Study of Temperature Adaptation in a Psychrophilic Enzyme, *J. Mol. Biol. 297*, 1015-1026.

51. Petrounia, I. P. and Arnold, F. H. (2000) Designed Evolution of Enzymatic Properties, *Curr. Opin. Biotechnol. 11*, 325-330.

52. Zhao, H. and Arnold, F. H. (1997) Optimization of DNA Shuffling for High Fidelity Recombination, *Nucleic Acids Res. 25*, 1307-1308.

53. Bornscheuer, U. T. and Pohl, M. (2001) Improved Biocatalysts by Directed Evolution and Rational Protein Design, *Curr. Opin. Chem Biol. 5*, 137-143.

54. Ghanem, E. and Raushel, F. M. (2005) Detoxification of Organophosphate Nerve Agents by Bacterial Phosphotriesterase, *Toxicol. Appl. Pharmacol. 207*, 459-470.

55. Gerlt, J. A. and Raushel, F. M. (2003) Evolution of Function in (Beta/Alpha)8-Barrel Enzymes, *Curr. Opin. Chem Biol. 7*, 252-264.

56. Benning, M. M., Kuo, J. M., Raushel, F. M., and Holden, H. M. (1994) 3-Dimensional Structure of Phosphotriesterase - An Enzyme Capable of Detoxifying Organophosphate Nerve Agents, *Biochemistry 33*, 15001-15007.

57. Benning, M. M., Hong, S. B., Raushel, F. M., and Holden, H. M. (2000) The Binding of Substrate Analogs to Phosphotriesterase, *J. Biol. Chem. 275*, 30556-30560.

58. Chen-Goodspeed, M., Sogorb, M., and Raushel, F. M. (1999) Determining Reactivity and Stereospecificity of Phosphotriesterase From Pseudonomas Diminuta by Site-Specific Mutagenesis, *Faseb Journal 13*, A1446.

59. Chen-Goodspeed, M., Sogorb, M. A., Wu, F. Y., Hong, S. B., and Raushel, F. M. (2001) Structural Determinants of the Substrate and Stereochemical Specificity of Phosphotriesterase, *Biochemistry 40*, 1325-1331.

60. Hong, S. B. and Raushel, F. M. (2004) Control of Stereoselectivity in Phosphotriesterase, *Protein Engineering 388*, 256-266.

61. Lai, K. H., Dave, K. I., and Wild, J. R. (1994) Bimetallic Binding Motifs in Organophosphorus Hydrolase Are Important for Catalysis and Structural Organization, *Journal of Biological Chemistry 269*, 16579-16584.

62. McDaniel C.S., McDaniel J., Wales M.E., and Wild J.R. (2006.) Biocatalytic Coatings, in *Paint & Coatings Industry 12*, 26-33.

63. LeJeune, K. E. and Russell, A. J. (1999) Biocatalytic Nerve Agent Detoxification in Fire Fighting Foams, *Biotechnology and Bioengineering 62*, 659-665.

64. Pei, L., Omburo, G., McGuinn, W. D., Petrikovics, I., Dave, K., Raushel, F. M., Wild, J. R., Deloach, J. R., and Way, J. L. (1994) Encapsulation of Phosphotriesterase Within Murine Erythrocytes, *Toxicology and Applied Pharmacology 124*, 296-301.

65. Russell, R. J., Pishko, M. V., Simonian, A. L., and Wild, J. R. (2000) Poly(Ethylene Glycol) Hydrogel-Encapsulated Fluorophore-Enzyme Conjugates for Direct Detection of Organophosphorus Neurotoxins, *Abstracts of Papers of the American Chemical Society 219*, U107.

66. Rainina, E. I., Efremenco, E. N., Varfolomeyev, S. D., Simonian, A. L., and Wild, J. R. (1996) The Development of a New Biosensor Based on Recombinant E-Coli for the Direct Detection of Organophosphorus Neurotoxins, *Biosensors & Bioelectronics 11*, 991-1000.

67. Constantine, C. A., Mello, S. V., Dupont, A., Cao, X., Santos, D., Jr., Oliveira ON Jr, Strixino, F. T., Pereira, E. C., Cheng, T. C., Defrank, J. J., and Leblanc, R. M. (2003) Layer-by-Layer Self-Assembled Chitosan/Poly(Thiophene-3-Acetic Acid) and Organophosphorus Hydrolase Multilayers, *J. Am. Chem. Soc. 125*, 1805-1809.

68. Richins, R. D., Mulchandani, A., and Chen, W. (2000) Expression, Immobilization, and Enzymatic Characterization of Cellulose-Binding Domain-

Organophosphorus Hydrolase Fusion Enzymes, *Biotechnology and Bioengineering 69*, 591-596.

69. Wang, J., Krause, R., Block, K., Musameh, M., Mulchandani, A., and Schoning, M. J. (2003) Flow Injection Amperometric Detection of OP Nerve Agents Based on an Organophosphorus-Hydrolase Biosensor Detector, *Biosensors & Bioelectronics 18*, 255-260.

70. Andreopoulos, F. M., Roberts, M. J., Bentley, M. D., Harris, J. M., Beckman, E. J., and Russell, A. J. (1999) Photoimmobilization of Organophosphorus Hydrolase Within a PEG-Based Hydrogel, *Biotechnology and Bioengineering 65*, 579-588.

71. White, B. J. and Harmon, H. J. (2005) Optical Solid-State Detection of Organophosphates Using Organophosphorus Hydrolase, *Biosensors & Bioelectronics 20*, 1977-1983.

72. Grimsley, J. K., Calamini, B., Wild, J. R., and Mesecar, A. D. (2005) Structural and Mutational Studies of Organophosphorus Hydrolase Reveal a Cryptic and Functional Allosteric-Binding Site, *Arch. Biochem. Biophys. 442*, 169-179.

73. Russell, A. J., Berberich, J. A., Drevon, G. E., and Koepsel, R. R. (2003) Biomaterials for Mediation of Chemical and Biological Warfare Agents, *Annual Review of Biomedical Engineering 5*, 1-27.

74. Pace, C. N. and Scholtz, J. M. (1997) Measuring the conformational stability of a protein, in *Protein Structure: A Practical Approach* 311-330 (T.E.Creighton, Ed.) Oxford University Press, London.

75. Di Sioudi, B. D., Miller, C. E., Lai, K., Grimsley, J. K., and Wild, J. R. (1999) Rational Design of Organophosphorus Hydrolase for Altered Substrate Specificities, *Chem. Biol. Interact. 119-120*, 211-223.

76. Di Sioudi, B. D., Grimsley, J. K., Lai, K., and Wild, J. R. (1999) Modification of Near Active Site Residues in Organophosphorus Hydrolase Reduces Metal Stoichiometry and Alters Substrate Specificity, *Biochemistry 38*, 2866-2872.

77. Arnold, U. and Ulbrich-Hofmann, R. (2001) Proteolytic Degradation of Ribonuclease A in the Pretransition Region of Thermally and Urea-Induced Unfolding, *European Journal of Biochemistry 268*, 93-97.

78. Jackson, C., Kim, H. K., Carr, P. D., Liu, J. W., and Ollis, D. L. (2005) The Structure of an Enzyme-Product Complex Reveals the Critical Role of a Terminal Hydroxide Nucleophile in the Bacterial Phosphotriesterase Mechanism, *Biochimica et Biophysica Acta-Proteins and Proteomics 1752*, 56-64.

79. Fraternali, F. and Cavallo, L. (2002) Parameter Optimized Surfaces (POPS): Analysis of Key Interactions and Conformational Changes in the Ribosome, *Nucleic Acids Research 30*, 2950-2960.

80. Hebert, E. J., Giletto, A., Sevcik, J., Urbanikova, L., Wilson, K. S., Dauter, Z., and Pace, C. N. (1998) Contribution of a Conserved Asparagine to the Conformational Stability of Ribonucleases Sa, Ba, and T1, *Biochemistry 37*, 16192-16200.

81. McGaughey, G. B., Gagne, M., and Rappe, A. K. (1998) Pi-Stacking Interactions. Alive and Well in Proteins, *J. Biol. Chem. 273*, 15458-15463.

82. Gallivan, J. P. and Dougherty, D. A. (1999) Cation-Pi Interactions in Structural Biology, *Proc. Natl. Acad. Sci. U. S. A 96*, 9459-9464.

83. Waters, M. L. (2002) Aromatic Interactions in Model Systems, *Curr. Opin. Chem. Biol. 6*, 736-741.

84. Waters, M. L. (2004) Aromatic Interactions in Peptides: Impact on Structure and Function, *Biopolymers 76*, 435-445.

85. Zacharias, N. and Dougherty, D. A. (2002) Cation-Pi Interactions in Ligand Recognition and Catalysis, *Trends Pharmacol. Sci. 23*, 281-287.

86. Carver, F. J., Hunter, C. A., Livingstone, D. J., Mccabe, J. F., and Seward, E. M. (2002) Substituent Effects on Edge-to-Face Aromatic Interactions, *Chemistry-A European Journal 8*, 2848-2859.

87. Kim, E., Paliwal, S., and Wilcox, C. S. (1998) Measurements of Molecular Electrostatic Field Effects in Edge-to-Face Aromatic Interactions and CH-Pi Interactions With Implications for Protein Folding and Molecular Recognition, *Journal of the American Chemical Society 120*, 11192-11193.

88. Zou, Q., Habermann-Rottinghaus, S. M., and Murphy, K. P. (1998) Urea Effects on Protein Stability: Hydrogen Bonding and the Hydrophobic Effect, *Proteins 31*, 107-115.

89. Puchkaev, A. V., Koo, L. S., and Ortiz de Montellano, P. R. (2003) Aromatic Stacking As a Determinant of the Thermal Stability of CYP119 From Sulfolobus Solfataricus, *Arch. Biochem. Biophys. 409*, 52-58.

VITA

Name: Tony Elvern Reeves

Address: MS 2128 Biochemistry Biophysics, Texas A&M University, College Station, TX 77843

Email Address: treeves@tamu.edu

Education: Ph.D. Biochemistry, Texas A&M University 2006
M.S., Biology, Tarleton State University 1999
B.S., Biology, Tarleton State University 1993